Physiologically-Based Pharmacokinetics of Lysosomotropic Chloroquine in Rat and Man

Xin Liu and William J. Jusko

Department of Pharmaceutical Sciences, School of Pharmacy and Pharmaceutical Sciences, State University of New York at Buffalo, Buffalo, New York

Running Title: PBPK Modeling of Chloroquine

Corresponding Author: William J. Jusko, Ph.D., Department of Pharmaceutical Sciences, School of Pharmacy and Pharmaceutical Sciences, 404 Pharmacy Building, State University of New York at Buffalo, Buffalo, NY, 14214, E-mail: wjjusko@buffalo.edu

Number of text pages: 22 (including Abstract)

Number of tables: 4

Number of figures: 7

Number of references: 60

Number of words:

    Abstract: 249

    Introduction: 742

    Discussion: 1527

ABBREVIATIONS: *GFR*, Glomerular Filtration Rate; IC_{50}, drug concentration causing 50% inhibition; NCA, Non-compartmental analysis; PBPK, physiologically-based pharmacokinetic.

Recommended Section: Metabolism, Transport, and Pharmacogenetics

ABSTRACT

A semi-mechanistic physiologically-based pharmacokinetic (PBPK) model for chloroquine (CQ), a highly lysosomotropic weak base, was applied to digitized rat (Adelusi and Salako, 1982a) and human (Frisk-Holmberg et al, 1984) concentration versus time data. The PBPK model in rat featured plasma and RBC concentrations, extensive and apparent nonlinear tissue distribution, fitted hepatic and renal intrinsic clearances, and a plasma half-life of about 1 day. Tissue to plasma CQ ratios at 50 h after dosing were highest in lung, kidney, liver, and spleen (182-318) and lower in heart, muscle, brain, eye, and skin (11-66). The RBC to plasma ratio of 11.6 was assumed to reflect cell lipid partitioning. A lysosome-based extended model was used to calculate subcellular CQ concentrations based on tissue mass balances, fitted plasma, interstitial, and free cytosol concentrations, and literature-based pH and pKa values. The CQ tissue component concentrations ranked: lysosome >> acidic phospholipid > plasma = interstitial = cytosol ≥ neutral lipids. The extensive lysosome sequestration appeared to change over time and was attributed to lowering pH values caused by proton pump influx of hydrogen ions. The man-to-rat volume of distribution (*Vss*) ratio of 7 used to scale rat tissue partitioning to man along with estimation of hepatic clearance allowed excellent fitting of oral dose PK (150-600 mg) of CQ with a 50-day half-life in man. The prolonged PK of chloroquine was well-characterized for rat and man with this PBPK model. The calculated intra-tissue concentrations and lysosomal effects have therapeutic relevance for CQ and other cationic drugs.

Significance Statement:

Sequestration in lysosomes is a major factor controlling the pharmacokinetics and pharmacology of chloroquine and other cationic drugs. This report provides comprehensive physiologic modeling of chloroquine distribution in tissues and overall disposition in rat and man revealing expected complexities and inferences related to its subcellular association with various tissue components.

Introduction

Chloroquine (CQ) is a classic anti-malarial agent that was identified in 1934, approved by the FDA in 1949, and features additional immunomodulatory, anti-viral, anti-cancer, and neurological activities (Savarino et al, 2002; Plantone and Koudriavtseva, 2018; Schrezenmeier and Dorner, 2020). The general pharmacological and pharmacokinetic (PK) properties of this 4-aminoquinoline compound are shared by hydroxychloroquine (HCQ) and several newer compounds (White, 1985).

The clinical pharmacokinetics of CQ have been extensively reviewed (White, 1985; Ducharme and Farinotti, 1996). In man, the drug is well-absorbed after oral doses of 150 to 600 mg, exhibits modest plasma protein binding (fraction unbound, fu is 0.40) (Walker et al, 1983), undergoes partial renal excretion with 70% of an oral dose excreted unchanged in urine, is partly metabolized by CYP2C8 and CYP3A4/5 enzymes to de-ethylated metabolites (McChesney et al., 1966, Kim, et al, 2003), and is enantiomeric with modest differences in disposition of its R- and S-forms. The mono-desethyl metabolite is also active. Most notable is its extensive tissue distribution having a steady-state volume of distribution (Vss) of about 800 L/kg and terminal half-life ($t_{1/2}$) of 30 to 60 days in man (Frisk-Holmberg et al, 1984; Moore et al, 2011). The strong tissue affinity and large Vss of CQ is attributed to lysosomal trapping of this lipophilic cation along with association with acidic phospholipids in cell membranes.

While there is little experimental data for CQ distribution in human tissues, there is extensive evidence for CQ distribution into various tissues of rats. Lysosomal uptake of CQ has been directly studied (Allison and Young, 1964; MacIntyre and Cutler, 1988, 1993; Tietz et al, 1990; Daniel et al, 1995; Zhang et al, 2011). The drug has often been used as a positive control for assessing lysosomal function and uptake of other moderate-to-strong bases (Cramb, 1986;

5

Myers et al, 1995; Ishizaki et al, 2000). The overall distribution of CQ into 10 tissues of rats over time was described (Adalusi and Salako, 1982a), but the data have not been analyzed by physiologically-based PK (PBPK) modeling. On the other hand, more limited tissue data for HCQ in rats was subjected to PBPK (Collins et al, 2018).

While it has long been recognized that lipophilic bases exhibit strong tissue binding and relatively large *Vss* values (Watanabi and Kozaki, 1978), it was not until 2002 that a PBPK perspective offered a tissue compositional concept for these drugs depicting the joint roles of ionization, lipid partitioning, pH differentials, and lysosomal trapping of ionized cations (Yokogawa et al, 2002). These ideas were later extended to consider diffusive movement of drug molecules within cell compartments (Trapp et al, 2008; Zheng et al, 2011). A more complete tissue composition-based model for such compounds was evolved (Assmus et al, 2017).

Software for operation of generic PBPK models (SimulationsPlus, SimCyp, PK-Sim) include general methods for estimating tissue-to-plasma partition coefficients (K_P) of various drugs based on chemical nature (acid, base, neutral), physicochemical properties (logP, pKa), the *fu* of the drug, and the partial tissue composition. Prediction methods for moderate-to-strong lipophilic bases include the lipid composition of various tissues (Rodgers et al, 2005). Such predictions are considered good when tissue-plasma ratios fall within 3-fold of known values. This approach was extended to include lysosomal trapping in lysosome-rich organs such as liver, kidney, and lung (Assmus et al, 2017). While compounds considered included propranolol and imipramine that are known (Cramb, 1986; Ishizaki et al, 2000) to trap in lysosomes of rats, none of the 9 antimalarial agents in clinical use (White, 1985; Trapp et al, 2008) were included. CQ differ from many others in being a divalent rather than monovalent base. Equations for K_p that include lysosomal trapping in some tissues are in the current SimulationsPlus (Lancaster, CA)

software.

With the extensive pre-clinical and human PK data available for CQ and the absence of detailed modeling, it is of interest to apply PBPK modeling to explore how the extensive lysosomal trapping explains in vivo PK. This report: 1.) Applies a generalized PBPK model to digitized data for CQ in various tissues of rats (Adelusi and Salako, 1982a); 2.) Scales the PBPK model to digitized data for CQ PK in man (Frisk-Holmberg et al, 1984); 3.) Adapts published equations (Rodgers et al, 2005; Assmus et al, 2017) for calculating tissue drug concentrations with lysosomal trapping; 4.) Considers the relevance of lysosomotropic effects of CQ (lysosomal changes in pH, volume, and lipids) on its PK; and 5.) Relates these assessments to the pharmacology of CQ and related compounds.

Materials and Methods

Data Analysis

The CQ concentration versus time data for plasma and tissues of rats (Adelusi and Salako 1982a), and blood CQ concentration versus time for man (Frisk-Holmberg et al, 1984) were obtained by digitization (Rodiovov, 2000). The blood from rats was obtained by cardiac puncture. Blood concentrations for man were converted to plasma concentrations using the authors' published relationship. The numerical data used are listed in Tables S1 and S2 in the Supplemental Materials.

Measured tissue CQ concentration ($C_{t(meas)}$) data of rat were corrected for assumed residual blood by first converting measured red blood cell (RBC) to plasma (C_{pl}) concentration ratios (K_b) to whole blood concentrations (C_{bl}):

$$C_{bl} = C_{pl} \cdot (1 + (K_b - 1) \cdot Hct) \tag{1}$$

The hematocrit (*Hct*) value of rat used was 0.4 (Lee and Blaufox, 1985). Then adjustments to

the corrected tissue concentrations (C_t) were made using:

$$C_t = \frac{C_{t(meas)} - C_{bl} \cdot (V_{vasc}/V_t)}{1 - (V_{vasc}/V_t)} \qquad (2)$$

where V_{vasc} and V_t are tissue vascular and total tissue volumes. Literature values for V_{vasc} were

from (Bernareggi and Rowland, 1991).

Tissue partition coefficients *Kp* were obtained by parameter estimation through PBPK modeling

as described in detail below. In addition, in silico *Kp* predictions were obtained for comparison

using GastroPlus™ PBPK Simulator (version 9.6.2, Simulations Plus Inc., Lancaster, CA) based

on published methods (Poulin and Theil, 2002), (Berezhkovskiy, 2004), (Rodgers and Rowland,

2006) and an adapted method (Assmus et al, 2017) in the software that includes lysosomal

trapping for basic compounds.

PBPK Model

Figure 1 shows the proposed general PBPK model structure for CQ. This model consists

of red blood cells (RBC), plasma, liver, kidney, lung, spleen, heart, brain, muscle, skin, eye and a

remainder compartment. The elimination pathway for CQ is partly hepatic metabolism and partly

renal clearance in rodents. Only CQ in plasma (not RBC) was assumed to access tissue spaces.

The renal clearance for CQ consisting of glomerular filtration (*GFR*) and active secretion was

fixed to two times *GFR*. Physiological parameter definitions and values are listed in Table 1 and

2. Plasma flow and tissue volumes were obtained from (Brown et al, 1997; Bernareggi and

Rowland, 1991).

A nonlinear total cytosol (*TC*) to cytosol water partition coefficient for CQ (Kp_{tissue}) was

applied due to variable concentration ratios between tissues and plasma. It was assumed that only

the free fraction of CQ from the interstitial space (*IS*) was available to cytosol and available for

apparent binding:

$$Kp_{tissue,u} = 1 + \frac{B_{max}}{C_{IS} + K_D} \tag{3}$$

where C_{IS} is the free concentration of CQ in interstitial space, B_{max} is the binding capacity for different tissues (µg/ml), and K_D is the equilibrium dissociation constant (µg/ml). A different K_D *(K_{D2})* was applied for skin (Olatunde, 1971), eye and muscle due to melanin binding of CQ in skin and eye and because muscle has a similar curve shape as skin.

The differential equations for various compartments of the PBPK model are:

Artery:

$$V_{artery} \cdot \frac{dC_{artery}}{dt} = Input1 + Q_{lung} \cdot \frac{C_{lung.IS}}{fu} - (Q_{liver} + Q_{kidney} + Q_{heart} + Q_{muscle} + Q_{skin} +$$

$$Q_{spleen} + Q_{brain} + Q_{eye} + Q_{rest}) \cdot C_{artery} - fu \cdot GFR \cdot C_{artery} \tag{4}$$

Vein:

$$V_{vein} \cdot \frac{dC_{vein}}{dt} = (Q_{liver} + Q_{spleen}) \cdot \frac{C_{liver.IS}}{fu} + Q_{kidney} \cdot \frac{C_{kidney.IS}}{fu} + Q_{heart} \cdot \frac{C_{heart,IS}}{fu} + Q_{muscle} \cdot$$

$$\frac{C_{muscle,IS}}{fu} + Q_{skin} \cdot \frac{C_{skin,IS}}{fu} + Q_{brain} \cdot \frac{C_{brain,IS}}{fu} + Q_{eye} \cdot \frac{C_{eye}}{Kp_{eye}} + Q_{rest} \cdot \frac{C_{rest}}{Kp_{rest}} - Q_{lung} \cdot C_{vein} \tag{5}$$

Liver:

$$V_{liver,IS} \cdot \frac{dC_{liver,IS}}{dt} = Input2 + Q_{liver} \cdot \left(C_{artery} - \frac{C_{liver,IS}}{fu}\right) + Q_{spleen} \cdot \left(\frac{C_{spleen,IS}}{fu} - \frac{C_{liver,IS}}{fu}\right) -$$

$$PS_1 \cdot \left(C_{liver,IS} - \frac{C_{liver,TC}}{Kp_{u,liver}}\right) \tag{6}$$

$$V_{liver,TC} \cdot \frac{dC_{liver,TC}}{dt} = PS_1 \cdot \left(C_{liver,IS} - \frac{C_{liver,TC}}{Kp_{u,liver}}\right) - CL_{u,int} \cdot \frac{C_{liver,TC}}{Kp_{u,liver}} \tag{7}$$

Kidney:

$$V_{kidney,IS} \cdot \frac{dC_{kidney.IS}}{dt} = Q_{kidney} \cdot \left(C_{artery} - \frac{C_{kidney,IS}}{fu}\right) - PS_2 \cdot \left(C_{kidney,IS} - \frac{C_{kidney,TC}}{Kp_{u,kidney}}\right) \tag{8}$$

$$V_{kidney,TC} \cdot \frac{dC_{kidney,TC}}{dt} = PS_2 \cdot \left(C_{kidney,IS} - \frac{C_{kidney,TC}}{Kp_{u,kidney}}\right) - CL_{k,int} \cdot \frac{C_{kidney,TC}}{Kp_{u,kidney}} \tag{9}$$

Heart:

$$V_{heart,IS} \cdot \frac{dC_{heart,IS}}{dt} = Q_{heart} \cdot \left(C_{artery} - \frac{C_{heart,IS}}{fu} \right) - PS_3 \cdot \left(C_{heart,IS} - \frac{C_{heart,TC}}{Kp_{u,heart}} \right) \tag{10}$$

$$V_{heart,TC} \cdot \frac{dC_{heart,TC}}{dt} = PS_3 \cdot \left(C_{heart,IS} - \frac{C_{heart,TC}}{Kp_{u,heart}} \right) \tag{11}$$

Lung:

$$V_{lung,IS} \cdot \frac{dC_{lung,IS}}{dt} = Q_{lung} \cdot \left(C_{vein} - \frac{C_{lung,IS}}{fu} \right) - PS_2 \cdot \left(C_{lung,IS} - \frac{C_{lung,TC}}{Kp_{u,lung}} \right) \tag{12}$$

$$V_{lung,TC} \cdot \frac{dC_{lung,TC}}{dt} = PS_2 \cdot \left(C_{lung,IS} - \frac{C_{lung,TC}}{Kp_{u,lung}} \right) \tag{13}$$

Spleen:

$$V_{spleen,IS} \cdot \frac{dC_{spleen,IS}}{dt} = Q_{spleen} \cdot \left(C_{artery} - \frac{C_{spleen,IS}}{fu} \right) - PS_2 \cdot \left(C_{spleen,IS} - \frac{C_{spleen,TC}}{Kp_{u,spleen}} \right) \tag{14}$$

$$V_{spleen,TC} \cdot \frac{dC_{spleen,TC}}{dt} = PS_2 \cdot \left(C_{spleen,IS} - \frac{C_{spleen,TC}}{Kp_{u,spleen}} \right) \tag{15}$$

Brain:

$$V_{brain,IS} \cdot \frac{dC_{brain,IS}}{dt} = Q_{brain} \cdot \left(C_{artery} - \frac{C_{brain,IS}}{fu} \right) - PS_3 \cdot \left(C_{brain,IS} - \frac{C_{brain,TC}}{Kp_{u,brain}} \right) \tag{16}$$

$$V_{brain,TC} \cdot \frac{dC_{brain,TC}}{dt} = PS_3 \cdot \left(C_{brain,IS} - \frac{C_{brain,TC}}{Kp_{u,brain}} \right) \tag{17}$$

Muscle:

$$V_{muscle,IS} \cdot \frac{dC_{muscle,IS}}{dt} = Q_{muscle} \cdot \left(C_{artery} - \frac{C_{muscle,IS}}{fu} \right) - PS_4 \cdot \left(C_{muscle,IS} - \frac{C_{muscle,TC}}{Kp_{u,muscle}} \right) \tag{18}$$

$$V_{muscle,TC} \cdot \frac{dC_{muscle,TC}}{dt} = PS_4 \cdot \left(C_{muscle,IS} - \frac{C_{muscle,TC}}{Kp_{u,muscle}} \right) \tag{19}$$

Skin:

$$V_{skin,IS} \cdot \frac{dC_{skin,IS}}{dt} = Q_{skin} \cdot \left(C_{artery} - \frac{C_{skin,IS}}{fu} \right) - PS_4 \cdot \left(C_{skin,IS} - \frac{C_{skin,TC}}{Kp_{u,skin}} \right) \tag{20}$$

$$V_{skin,TC} \cdot \frac{dC_{skin,TC}}{dt} = PS_4 \cdot \left(C_{skin,IS} - \frac{C_{skin,TC}}{Kp_{u,skin}} \right) \tag{21}$$

10

Eye:

$$V_{eye} \cdot \frac{dC_{eye}}{dt} = Q_{eye} \cdot \left(C_{artery} - \frac{C_{eye}}{Kp_{eye}} \right) \tag{22}$$

Remainder:

$$V_{rest} \cdot \frac{dC_{rest}}{dt} = Q_{rest} \cdot \left(C_{artery} - \frac{C_{rest}}{Kp_{rest}} \right) \tag{23}$$

where interstitial volume $(V_{i,IS})$, intracellular volume $(V_{i,TC})$, IS concentration $(C_{i,IS})$ TC concentration $(C_{i,TC})$, plasma flow (Q_i) and partition coefficients $(Kp_{u,i})$ are applied for tissue i; $CL_{u,int}$ and $CL_{k,int}$ are the unbound intrinsic clearances in liver and kidney; and PS_{1-4} are the permeability coefficients between interstitial and cell spaces. Assuming 1 g/mL tissue density: V_{rest} = body weight – summation of volumes for listed tissues, plasma and RBC; Q_{rest} = cardiac plasma output - summation of plasma flows for listed tissues.

The CQ concentrations in RBC and plasma were related as the partition coefficient (K_b):

$$C_{RBC} = K_b \cdot C_{plasma} \tag{24}$$

The dosing input for intraperitoneal (IP) dosing of CQ in rats was:

$$\frac{dA_{IP}}{dt} = -\left(ka_{plasma} \cdot fd \cdot A_{IP} + ka_{liver} \cdot (1 - fd) \cdot A_{IP} \right) \qquad A_{IP}(0) = Dose \tag{25}$$

$$Input1 = ka_{plasma} \cdot fd \cdot A_{IP} \tag{26}$$

$$Input2 = ka_{liver} \cdot (1 - fd) \cdot A_{IP} \tag{27}$$

where fd is the dose fraction directly entering plasma that was fixed to 0.1.

For human data, the systemic renal clearance $(CL_{s,kidney})$ was set as 70% of total systemic clearance $(CL_{s,total})$ calculated based on non-compartmental analysis (NCA) of the plasma data and intrinsic hepatic clearance $(CL_{u,int})$ was fitted. The connectivity of systemic $(CL_{s,total})$ and intrinsic clearances was assessed using:

$$CL_{s,total} = Q_{liver} \cdot \frac{fu \cdot CL_{u,int}}{Q_{liver} + fu \cdot CL_{u,int}} + Q_{kidney} \cdot \frac{fu \cdot CL_{k,int}}{Q_{kidney} + fu \cdot CL_{k,int}} + fu \cdot GFR \tag{28}$$

The oral dosing input of CQ in humans in place of *Input2* in Eq. 6 is:

$$Input = ka_{plasma} \cdot A_{PO} \qquad A_{PO}(0) = F \cdot Dose \qquad\qquad (29)$$

where the bioavailability (*F*) of CQ was assumed to be 1.0 (Frisk-Holmberg et al, 1984) and free

fraction of plasma (*fu*) for man is 0.4 (Ducharme and Farinotti, 1996).

The initial conditions for all differential equations are equal to 0 except for the dosing sites.

Extended Lysosome Model

The lysosome model (Figure 2) was adapted from (Assmus et al, 2017, Rodgers et al,

2005) and based on assumptions that: (1) only neutral molecules diffuse through the lysosome

membrane; (2) IS and cytosol concentrations are in *PS*-determined equilibrium with plasma

concentrations; (3) neutral drug equilibrium occurs between lysosome and cytosol

concentrations; (4) plasma and IS pH = 7.4, cytosol pH = 7.0, initial lysosome pH= 4.6, and

lysosome pH= 5 at 10 h; (5) only neutral molecules bind to neutral lipids (NL) and neutral

phospholipids (NP) while ionized drug binds to acidic phospholipids (AP).

The equations for the extended lysosome model are based on the mass balance:

$$C_{tissue} = f_{lyso} \cdot C_{lyso} + f_{cyto} \cdot C_{cyto} + f_{IS} \cdot C_{IS} + f_{NL} \cdot C_{NL} + f_{NP} \cdot C_{NP} + f_{AP} \cdot C_{AP} \qquad\qquad (30)$$

where C_{tissue} *and* C_{IS} are total tissue and interstitial CQ concentrations fitted using the PBPK

model, C_{lyso}, C_{cyto}, $C_{NL,}$ $C_{NP,}$ and C_{AP} are CQ concentrations associated with lysosomes, cytosol,

neutral lipids, neutral phospholipids, and acidic phospholipids, while *fi* are volume fractions of

total tissue for corresponding components. The following approach was applied for each tissue as

adapted from (Assmus et al, 2017) with assigned parameters from (Rodgers et al, 2005):

The C_{cyto} are calculated from the fitted C_{TC} profiles using the partition coefficients:

$$C_{cyto} = \frac{C_{TC}}{Kp_{\,u,tissue}} \qquad\qquad (31)$$

The C_{NL} and C_{NP} concentrations are calculated using the published *n*-octanol-to-water

partition coefficient (LogP = 4.63) (Lullmann and Wehling, 1979).

$$C_{NL} = C_{cyto} \cdot P \cdot Fn_{cyto} \tag{32}$$

$$C_{NP} = C_{cyto} \cdot (0.3 \cdot P + 0.7) \cdot Fn_{cyto} \tag{33}$$

where Fn_i are neutral CQ fractions in cytosol calculated from the known pKa values for the

divalent CQ (Trapp et al, 2008):

$$Fn_i = \frac{C_{i,neutral}}{C_{i,total}} = (1 + 10^{pKa1-pH_i} + 10^{pKa1+pKa2-2\cdot pH_i})^{-1} \tag{34}$$

where i is either plasma, lysosome or cytosol.

The C_{AP} concentrations of CQ were calculated using the association constant (Kap):

$$C_{AP} = Kap \cdot AP \cdot C_{cyto} \cdot (1 - Fn_{cyto}) \tag{35}$$

where AP are tissue concentrations of acidic phospholipids and Kap was calculated from the

$Kp_{u,RBC}$ using (Rodgers et al, 2005):

$$Kap = \frac{Kp_{u,RBC} - \frac{f_{cyto} \cdot Fn_{PL}}{Fn_{cyto}} - (P \cdot f_{nl} + (0.3 \cdot P + 0.7) \cdot f_{np}) \cdot Fn_{PL}}{AP \cdot \left(\frac{1}{Fn_{cyto}} - 1\right) \cdot Fn_{PL}} \tag{36}$$

where $Kp_{u,RBC} = K_b/fu = 29$ and fu is the free fraction of drug in plasma.

The CQ concentrations in lysosomes in relation to C_{cyto} are governed by equilibration of

the neutral molecules and pH-partitioning:

$$C_{lyso} = C_{cyto} \cdot \frac{Fn_{cyto}}{Fn_{lyso}} \tag{37}$$

It was assumed that the pH of lysosome is 5 at 10 h for all tissues. With initial

substitution of $f_{AP} = (1 - f_{NL} - f_{IS} - f_{NP} - f_{cyto} - f_{lyso})$, Eq. 30 was re-arranged to calculate the

effective volume fraction f_{lyso} for all tissues using:

$$f_{lyso} = \frac{C_{tissue} - C_{cyto} \cdot f_{cyto} - C_{IS} \cdot f_{IS} - C_{NP} \cdot f_{NP} - C_{NL} \cdot f_{NL} - (1 - f_{NL} - f_{IS} - f_{NP} - f_{cyto}) \cdot C_{AP}}{C_{lyso} - C_{AP}} \tag{38}$$

where C_{tissue} are total CQ tissue concentrations fitted with the PBPK model. Then, assuming f_{lyso}

13

is constant, the pH of lysosomes for each time point was calculated using:

$$C_{lyso} = \frac{C_{tissue} - C_{cyto} \cdot f_{cyto} - C_{IS} \cdot f_{IS} - C_{NL} \cdot f_{NL} - C_{NP} \cdot f_{NP} - (1 - f_{lyso} - f_{NL} - f_{IS} - f_{NP} - f_{cyto}) \cdot C_{AP}}{f_{lyso}} \tag{39}$$

$$Fn_{lyso} = C_{cyto} \cdot \frac{Fn_{cyto}}{C_{lyso}} \tag{40}$$

$$pH = log\left(\frac{-10^{pKa1} - \sqrt{(10^{pKa1})^2 - 4*\left(1 - \frac{1}{Fn_{lyso}}\right)*10^{pKa1+pKa2}}}{2*\left(1 - \frac{1}{Fn_{lyso}}\right)}\right) \tag{41}$$

where Eq. 41 was derived by re-arranging Eq. 34.

The modeling was performed in stages. First, Eq. 3 – 27 were applied to fit the rat PBPK plasma and tissue data and generate C_{tissue}, C_{IS} and C_{TC} concentrations over time. This assumes that the nonlinear tissue binding reflects overall lipid partitioning and lysosomal trapping of CQ. Then, the lysosome model (Eq. 30-39) was used to calculate the theoretical lipid and lysosome concentrations of CQ followed by generation of apparent pH values over time for each tissue (Eq. 39-41). Subsequently, the PBPK model was applied to fit the human PK data. Lastly, the tissue subcomponent model was applied to the human PK using literature values for lipid components in man (Rogers et al, 2005).

Model Fitting

For rat data, estimated were: binding capacity (B_{max}) and equilibrium dissociation constants (K_{D1} and K_{D2}) comprising the apparent partition coefficients (Kp) for all tissues, permeability coefficients (PS_{1-4}), two CQ absorption rate constants (ka_{plasma} and ka_{liver}), and the hepatic intrinsic clearance ($CL_{u,int}$). For human data, ka_{plasma}, $K_{D1,}$ and intrinsic hepatic clearance ($CL_{u,int}$) were estimated. All fittings and simulations were implemented using ADAPT 5 (Biomedical Simulations Resource, University of Southern California, Los Angeles, CA) using maximum likelihood estimation. The model was evaluated based on visual inspection of the

fitted profiles and CV% of parameter estimates. The variance model was: $V_i = (\sigma_1 + \sigma_2 \cdot Y_i)^2$ where V_i represents the variance of the ith data point, Y_i is the ith model prediction, and σ_1 and σ_2 are variance model parameters. Figures were created using GraphPad Prism 8.42 (GraphPad Software, La Jolla, CA). The PBPK model code is provided in the Supplemental Materials.

Results

Whole-body pharmacokinetics of CQ for rat

Figure 3 shows the measured CQ concentration in plasma and tissues from (Adelusi and Salako, 1982a) along with the PBPK model-fitted time-course profiles after single IP dosing. The highest drug concentrations are found in liver, lung, spleen and kidney. Heart, brain, and eye had intermediate concentrations and the others were much lower. The plasma and RBC concentrations were parallel, which supported use of a linear K_b constant. Generally, the PBPK model captures the plasma, RBC, and tissue PK very well. Blood in rats was obtained by cardiac punctures and thus was a mixture of arterial and venous blood. It was necessary to assume that this represented arterial concentrations, but use of mixed venous blood concentrations is commonplace in many PBPK models. The sampling site is only likely to make a difference for drugs with much more rapid distribution kinetics than CQ (Huang and Isoherranen, 2020).

The fitted parameters for each tissue obtained from model-fitting are listed in Table 2. Most parameters were estimated with good precision as indicated by the CV% values. The tissue-to-plasma ratios and Kp values for all tissues exceed 1.0 after the absorption/distribution phase and varies among the tissues. The tissue-to-plasma ratios increase over time, but at 50-h are 318 for liver, 275 for lung, 267 for spleen, 182 for kidney, and 66 for heart, indicating extensive distribution of CQ. The B_{max} and K_D account for the variable Kp values that create the

15

non-parallel decline of tissue versus plasma concentrations and produce higher tissue to plasma

ratios as time progresses (Table 2). The B_{max} values were specific for each tissue, but two groups

of K_D values provided good fittings across the array of tissues. These were optimized by trial-

and-error seeking the most parsimonious sets of parameters. The tissues with the highest CQ

concentrations had the higher B_{max} values as expected. The permeability component of the model

was applied to all tissues except eye and remainder; the inclusion of PS_{1-4} significantly improved

the up-curve shapes of all organs at the early time periods compared to fittings without this

parameter. These up-curves varied somewhat and optimal fittings were obtained by using four

different PS values with liver exhibiting the highest PS value and brain the lowest as expected

(Jeong et al, 2017). The K_{D2} values were associated with the tissues with the least CQ uptake.

For optimal fittings, it was necessary to separate the IP dosing into two routes, 90% into

liver and 10% into plasma with 100% bioavailability, so two different ka values were applied,

slower into liver and faster into plasma. It seemed reasonable that a small part of the dose could

be absorbed systemically. Renal clearance consisting of passive filtration ($f_u \cdot GFR$) and active

transport along with hepatic clearance ($CL_{u,int}$) are responsible for CQ clearance. The systemic

renal clearance (630 mL/h/kg) was fixed to 2 times GFR (Grundmann et al, 1972). The GFR was

handled as direct removal from arterial plasma (Eq. 4) as the very high kidney concentrations

complicated its attachment to Eq. 8. The model-estimated hepatic intrinsic clearance was 11,600

mL/h/kg and exhibited the highest CV% (70.3) of all parameters. All other values were less than

36%. Based on systemic clearances obtained using Eq. 28, the kidney accounts for 29.7% of CQ

disposition and the liver 70.3%, in agreement with findings that 26- 47% of the dose was

excreted unchanged in urine of rats (Grundmann et al, 1972).

Table 2 lists the tissue-to-plasma ratios of CQ at times 10, 50, and 150 h to demonstrate the range of values as well as their time-dependence. The table also lists expected *Kp* values using three methods that do not include lysosomal uptake and one that does (Method 4). Methods 1-3 that include lipid binding as the major factor predict the early tissue-to-plasma ratios of CQ reasonably well only for those tissues with low lysosomal content. Method 4, which includes lysosomal uptake, reasonably predicts CQ values in most tissues except for muscle and skin. Methods such as Eq. 32 -36 are theoretical based on reasonable physiologic and physicochemical principles and the measured composition of tissues. However, they are very general and supported only by use of predictions of tissue-to-plasma ratios (*Kp*) of a variety of drugs (Rodgers et al, 2005; Assmus et al, 2017). Agreement between measured and predicted *Kp* values with such equations is inexact, usually within 2- or 3-fold as occurs with the results in Table 2. Direct in vivo measurement of drug associated with subcellular components requires imaging, which is difficult with whole tissues, and for drugs that are neither labeled nor fluoresce.

The basic PBPK model for CQ relies on digitized plasma concentrations and calculated tissue-to-plasma ratios (Adalusi and Salako, 1982a) and are thus close but inexact. However, the PBPK model-predicted descriptors of these concentrations such as *Cmax*, *Tmax*, and half-life are in reasonable concordance with the published values (see Supplemental Materials).

Extended lysosome model of CQ for rat

Figure 2 shows the structure of the multi-component lysosome model based on (Assmus et al, 2017) that was applied to the CQ tissue data. Table 3 lists the parameters and sources that were employed in Eq. 32-39 to calculate the subcellular concentrations of CQ. It was necessary to assume a pH of 5.0 at 10 h leading to a starting and eventual steady-state lysosomal pH of 4.6 for all tissues. It is cautioned that there could be a range of pH values in lysosomes distributed in

17

cells and among various tissues (Schmitt et al, 2019). Figure 4 shows calculated lysosome, cytosol, IS, neutral lipid, neutral phospholipid, and acidic phospholipid CQ concentration versus time profiles in all of the 8 tissues except eye along with the corresponding measured tissue concentrations. The lysosome concentrations are far higher than all others as governed by the pH gradient between lysosomes and cytosol. There is markedly greater ionization of CQ at the lower pH as indicated by the lower *Fn* values in Table 3. The acid phospholipids (AP) as governed by the *Kap* of 8.52 g/mg and high degree of ionization of CQ have the next highest CQ concentrations. The NL and NP concentrations of CQ are very low in spite of the relatively high logP of 4.63 owing to their access to only the neutral form of CQ for which the *Fn* is extremely low. The free drug in plasma, IS concentrations, and cytosol water concentrations are generally similar as these are equilibrating entities in the PBPK model. The cytosol and IS concentrations overlap in all tissues except liver and kidney where the cytosol concentrations are lower because of the clearance processes.

Figure 5 shows the calculated pH values in lysosomes in various tissues over time. It is assumed that the lysosome pH starts at a low value before CQ dosing, initially rises to higher values owing to influx of CQ, and slowly returns toward a baseline value of 4.6 with influx of hydrogen ions by the proton pump mechanism (Ishizaki et al, 2000; Ishida et al, 2013). This diminishment in lysosomal pH over time causing more uptake of CQ is the model-assigned reason for the increasing tissue-to-plasma ratios of CQ (Table 2).

An additional set of plasma and tissue data for CQ in rats (Adalusi and Salako, 1982b) was used to evaluate predictability of the basic PBPK model. Good concordance was found as shown in the Supplementary Materials.

Pharmacokinetics of CQ in man

18

The human PBPK model employed physiological parameters for man (Table 1), adjusted partition coefficients (from Table 2) based on the man-to-rat V_{ss} ratio, and fitted values of hepatic intrinsic clearance ($CL_{u,int}$), dissociation constant (K_{D1}) and ka_{plasm} (Table 4). Figure 6 shows excellent fittings of the 150, 300, 600 mg doses of CQ over the full time-course and parameter CV% values were very small. Oral absorption was relatively rapid producing the early high CQ concentrations.

The noncompartmental V_{ss} for man is 7 times that of rat, averaging 820 L/kg in man (Frisk-Holmberg et al, 1984) and (our calculated) 113 L/kg in rat (Adelusi and Salako, 1982a); thus we set R equal to 7.0 as an adjustment factor for multiplying rat Kp values. It was reported that 70% unchanged CQ is excreted by kidney in man (McChesney et al, 1966); hence the $CL_{s,kidney}$ was fixed to 70% of $CL_{s,total}$ that was estimated using NCA, and $CL_{u,int}$ was estimated by fitting the human data. The $CL_{u,int}$ is 1060 mL/h/kg, which results in $CL_{s,total}$ (722 ml/h/kg) similar to a reported value (Fisk-Holmberg et al, 1984).

Figure 7 shows the model-predicted CQ concentrations associated with all of the tissue components for four major tissues in man after the 600 mg dose. These were calculated based on published lipid contents for man (Table 3), but rat lysosomal fractions were employed. While the rank order of concentrations appears similar to those in rats (Figure 4), lysosomal concentrations were relatively higher in man. For example, in man lysosome-to-plasma CQ ratios at 1000 h were: 25054 for liver, 39654 for kidney, 56608 for lung, and 208976 for muscle. Corresponding values for rat at 50 h were: 3380, 8110, 8160, and 8530.

Discussion

Justification of the PBPK Model

The properties of chloroquine (CQ) are well-appreciated as it has been in clinical use since the 1950's and is a frequent probe for lysosomal functioning. Comprehensive reviews of its PK and pharmacology are available (White, 1985; Browning, 2014). The plasma and whole blood PK of CQ have been studied in several species and clearances were shown to scale allometrically (Moore et al, 2011).

The avid uptake of CQ into the liver, kidney, spleen, and lungs, which have abundant lysosomes, and lesser distribution to muscle and other tissues has been well-appreciated from other studies in rats (McChesney et al, 1965, 1967; Grundmann et al, 1972; Osifo, 1980), but the present data provide the most comprehensive view of the overall PK and tissue distribution of CQ in any species. The present PBPK modeling utilizes a two-stage approach, first generally assessing the array of 10 tissues and blood with classical PBPK modeling concepts, including apparent nonlinear tissue distribution. This provided estimates of CQ concentrations in IS and cell cytosol with the nonlinear component assumed to reflect CQ concentrations associated with various lipids and lysosomes. A complex distribution model for lipid binding and lysosome distribution (Assmus et al, 2017) was then adapted to allocate the total tissue concentrations of CQ into its subcomponents.

There is considerable evidence for lysosomal tissue distribution of CQ in rats supporting our PBPK modeling. The fluorescence of CQ facilitated early viewing of its high concentrations in intracellular lysosomes of cells (Allison and Young, 1964). Differential centrifugation and electrophoresis methods allowed measurement of the slow uptake of CQ into the hepatic lysosomes of rats dosed with CQ along with its inhibition of phospholipase A (Hostetler et al, 1985). Isolated rat hepatocytes demonstrated both uptake and metabolism of CQ, including marked reduction of uptake by ammonium chloride, a lysosomal inhibitor that alters lysosomal

20

pH (MacIntyre and Cutler, 1993). Their application of a cellular PK model argued that the permeability of the lysosomal membrane is rate limiting for hepatocyte uptake of CQ. A more complex model (similar to Figure 2) for the lysosomal uptake of CQ was developed for cells in culture (Trapp et al, 2008; Zheng et al, 2011). This process is mimicked by the simpler diffusion step (*PS*) between IS and cell content applied in our PBPK model (Figure 1) to account for the slow early rise in CQ concentrations in many tissues (Figure 3). The in vitro binding of CQ to various individual polar phospholipids has been measured (Lullmann and Wehling, 1979). The apparent partition coefficient of CQ for phosphotidylcholine was about 77 consistent with our AP-to-plasma ratios, and a *Kap* of about 2.0 g/mg, near to our *Kap* of 8.52 g/mg. Such in vitro binding was nonlinear for CQ and other compounds studied.

The nonlinear *Kp* in our basic PBPK model was used initially to account for the increases in tissue- to-plasma concentrations of CQ over time (Figure 3, Table 2). This may actually reflect a time-dependent process. Part of the lysosomotropic effects of CQ is the inhibition of phospholipid degradation (Hostetler et al, 1985). Use of isolated hepatocytes showed that acute exposure to CQ produces an increased lysosomal pH attributed to proton consumption (Tietz et al, 1990; Myers et al, 1995). Imaging of canine kidney cells has demonstrated phospholipidosis accompanied by altered vesicular pH and increased vesicle volume (Zhang et al, 2011). Our modeling (Figure 5) assumed that CQ produced, within hours of dosing, a rise in lysosome pH that slowly returned to the baseline owing to both elimination of CQ and influx of H^+ ions by the proton pump mechanism responsible for maintaining the normal low pH of 4 to 5. It is possible that phospholipodosis and increased vesicle volume also contribute to changing tissue-to-plasma ratios after CQ dosing (Table 2).

CQ exhibits strong binding to melanin, particularly in the eye (Schroeder and Gerber, 2014). This is implicated in ocular toxicity. The rat eye has modest concentrations of CQ (Figure 3, Table 2) and a small B_{max}. Melanin binding is saturable in vitro and the eye accounts for a very small fraction of CQ in the body.

The present effort was partly inspired by a publication describing the PBPK modeling of HCQ using data obtained from mice, many similar stated concepts, and with extrapolation to man (Collins et al, 2018). However, their modeling is based on only 4 tissues (blood, liver, kidney, and gut), while CQ studies offer much richer data. The authors did not provide their full array of equations utilized and their extrapolations to man do not cover the very long half-life known for HCQ (Tett et al, 1988).

Pharmacokinetics of Chloroquine in Man

The plasma concentration versus time courses of CQ in man for the 3 dose levels were well-captured with the PBPK model with 3 parameters needing customization (Figure 6, Table 4). These data are representative of many studies of CQ PK in man (Moore et al, 2011). Multiplying the rat Kp values by the man-to-rat Vss ratio of 7 was key. In turn, this implies that the total tissue and lysosomal concentrations of CQ are 7-fold higher in man than rat (Figure 7). This is supported by measurements of CQ showing skin-to-plasma ratios of about 34 at 48 hour after an IV dose in patients (Olatunde, 1971), while the 10-h skin ratio was 5.77 in rats (Table 2). Another cationic anti-malarial quinoline, HCQ, exhibits a Vss value that is 5.7-fold higher in man (86 L/kg) than in rats (15 L/kg) based on blood concentrations (Tett et al, 1988; Emami et al, 1998). It is possible that lysosomal pH is lower in man to produce greater sequestration of these drugs. Larger lysosomal volumes and greater acidic phospholipid content may be contributory.

On the other hand, *Vss* values for 10 other basic drugs are similar in man and rat (Sawada et al, 1984).

Therapeutic Implications of the PBPK Model

There are many therapeutic dosing regimens for CQ typically ranging 100 to 600 mg per day (Browning, 2014). The human data in Figure 6 reflects this range. The mechanism of action of CQ in malaria is thought to be its lysosomotropic effect on the acidic food vacuoles of the parasite increasing pH and interfering with the digestive degradation of hemoglobin in RBC.

Drugs such as CQ and HCQ are also used for treatment of patients with rheumatoid arthritis (RA) and systemic lupus erythematosus (SLE). Their myriad effects are attributed to interference of antigen processing in macrophages, down-regulation of immune responses, alteration of signaling pathways and transcriptional activity, and inhibition of cytokine production (Fox, 1993; Schrezenmeier and Dorner, 2020). While the lysosomotropic effects of CQ are stated to be most important clinically, more than 20 additional actions contributing to both therapeutic and adverse effects have been cited (Browning, 2014). There is current interest in using HCQ for autophagy modulation, the natural metabolic digestion of cell proteins and other materials in lysosomes; up-regulation of this process is a resistance mechanism for some tumors (Shi et al, 2017).

Our PK modeling predicts that CQ concentrations in the cytosol will be very low, similar to free drug concentrations in plasma and IS (Figures 4 and 7). However, multiple actions of CQ appear connected to or are triggered by the changes in lysosomal pH and associated alterations in lysosomal and cellular functions that ensue. The pharmacology of CQ and other lysosomotropic drugs is far more complex than can be explained by the very low unbound concentrations that are commonly thought to drive actions of many drugs. Some in vitro screening systems for drug

activity may not invoke the same lysosomal triggers. For example, the IC_{50} for CQ inhibition of mitogen-induced human lymphocyte proliferation is 19.5 μM or about 6.4 μg/mL (Kamal and Jusko, 2004), an in vitro system that is meaningful for immune effects of corticosteroids. This concentration is far above peak exposures of 0.1 μg/mL after 600 mg doses of CQ (Figure 6). Yet CQ is effective at these doses for treatment of patients with RA and SLE.

Of current interest, CQ and HCQ were found active in inhibiting SARS-CoV-2 in vitro with IC_{50} concentrations of around 6 μM (Liu et al, 2020). These too are well above typical therapeutic plasma concentrations. It can be questioned whether these in vitro responses are relevant in vivo and whether a lysosomotropic mechanism is present in some cell cultures. It has been argued that the lysosomotropic effects could partly make CQ effective as an anti-viral agent (Savarino et al, 2003; Plantone and Koudriavtseva, 2018). Some viruses enter their target cells by endosomes that merge into lysosomes. The low pH and action of enzymes liberates infectious nucleic acids from virus particles. Raising the lysosomal pH thus interferes with this process. However, recent attempts to use CQ and HCQ to treat COVID-19 viral infections have not shown efficacy and risk various toxicities (Qaseem et al, 2020).

This report demonstrates application of state-of-the-art PBPK modeling concepts, methods, and insights for an old drug with highly interesting tissue distribution and mechanisms of action. The principles underlying this modeling approach will likely be relevant to other cationic drugs that sequester in lysosomes, although their physicochemical properties and degree of changes in lysosome pH and structure may require more specific adjustments.

Acknowledgments

We appreciate the review of this manuscript by Dr. Viera Lucakova from SimulationsPlus.

Authorship Contributions

Participated in research design: Liu and Jusko

Conducted experiments: Not applicable.

Performed data analysis: Liu

Wrote or contributed to the writing of the manuscript: Liu and Jusko

References

Adelusi SA and Salako LA (1982a) Kinetics of the distribution and elimination of chloroquine in the rat. *Gen Pharmacol* 13:433-437.

Adalusi SA and Salako LA (1982b). The effect of protein-energy malnutrition on the absorption, distribution and elimination of chloroquine in the rat. *General Pharmacol* 13: 505–509.

Allison AC and Young MR (1964) Uptake of dyes by living cells in culture, Life Sciences 3:1407-1414.

Assmus F, Houston JB and Galetin A (2017) Incorporation of lysosomal sequestration in the mechanistic model for prediction of tissue distribution of basic drugs. *Eur J Pharm Sci* 109:419-430.

Berezhkovskiy LM (2004) Volume of distribution at steady state for a linear pharmacokinetic system with peripheral elimination. *J Pharm Sci* 93:1628-1640.

Bernareggi A and Rowland M (1991) Physiologic modeling of cyclosporin kinetics in rat and man. *J Pharmacokinet Biopharm* 19:21-50.

Brown RP, Delp MD, Lindstedt SL, Rhomberg LR and Beliles RP (1997) Physiological parameter values for physiologically based pharmacokinetic models. *Toxicol Ind Health* 13:407-484.

Browning DJ (2014) Pharmacology of Chloroquine and Hydroxychloroquine. In: Hydroxychloroquine and Chloroquine Retinopathy. Springer, New York, NY. https://doi.org/10.1007/978-1-4939-0597-3_2.

Collins KP, Jackson KM, and Gustafson DL (2018) Hydroxychloroquine: A physiologically-based pharmacokinetic model in the context of cancer-related autophagy modulation, *J Pharmacol Exp Ther* 365: 447-459.

Cramb G (1986) Selective lysosomal uptake and accumulation of the beta-adrenergic antagonist propranolol in cultured and isolated cell systems. *Biochem Pharmacol* 35: 1365-1372.

Davies B and Morris T (1993) Physiological parameters in laboratory animals and humans. *Pharm Res*. 10(7):1093-5

Daniel M. Syrek M, Janczar L and Boksa J (1995) The pharmacokinetics of promazine and its metabolites after acute and chronic administration to rats - A comparison with the pharmacokinetics of imipramine. *Pol J Pharmacol*. 47: 127-136.

Ducharme J and Farinotti R (1996) Clinical pharmacokinetics and metabolism of chloroquine: Focus on recent developments. *Clinical Pharmacokin* 31: 257-274.

Emami J, Pasutto FM and Jamali F (1998) Effect of experimental diabetes mellitus and arthritis on the pharmacokinetics of hydroxychloroquine enantiomers in rats. *Pharm Res* 15:897-903.

Feke GT, Tagawa H, Deupree DM, Goger DG, Sebag J, and Weiter JJ (1989) Blood flow to the normal human retina. *Invest Ophthamol Vis Sci* 30: 58-65.

Fox RJ (1993) Mechanism of action of hydroxychloroquine as an antirheumatic drug, *Sem Arthritis Rheumatism*. 23: 82-91.

Frisk-Holmberg M, Bergqvist Y, Termond E and Domeij-Nyberg B (1984) The single dose kinetics of chloroquine and its major metabolite desethylchloroquine in healthy subjects. *Eur J Clin Pharmacol* 26:521-530.

(2019) GastroPlus Manual, Simulations Plus, Inc, 42505 10th Street West, Lancaster, California.

Geng Y, Greenberg KP, Wolfe R, Gray DC, Hunter JJ, Dubra A, Flannery JG, Williams DR and Porter J (2009) In vivo imaging of microscopic structures in the rat retina. *Invest Ophthalmol Vis Sci* 50:5872-5879.

Grundmann M, Mikulikrova I and Vrublovsky P (1972) Tissue distribution of chloroquine in rats in the course of long-term application. *Arch Int Pharmacodyn Ther* 197:45-52.

Hostetler KY, Reasor M, and Yazaki PJ (1985) Chloroquine-induced phospholipid fatty liver. Measurement of drug and lipid concentrations in rat liver lysosomes, *J Biol Chem* 260: 215-219.

Huang W and Isoherranen N (2020) Sampling site has a critical impact on physiologically based pharmacokinetic modeling, J Pharmacol Exp Ther 372: 30-45.

Ishida Y, Nayak S, Mindell JA and Grabe M (2013) A model of lysosomal pH regulation. *J Gen Physiol* 141:705-720.

Ishizaki J, Yokogawa K, Ichimura F, and Ohkuma S (2000) Uptake of imipramine in rat liver lysosomes in vitro and its inhibition by basic drugs, *J Pharmacol Exp Ther* 294: 1088 – 1098.

Jeong Y-S, Yin C-S, Ryu H-M, Noh C-K, Song Y-K, and Chung S-J (2017) Estimation of the minimun permeability coefficient in rats for perfusion-limited tissue distribution in whole-body physiologically-based pharmacokinetics, Eur J Pharmaceut Biopharm 115: 1-17.

Kamal MA and Jusko WJ (2004) Interactions of prednisolone and other immunosuppressants used in dual treatment of systemic lupus erythematosus in lymphocyte proliferation assays. J Clin Pharmacol, 44:1034-45.

Kim K-A, Park J-Y, Lee J-S, and Lim S (2003) Cytochrome P-450 2C8 and CYP3A4/5 are involved in chloroquine metabolism in human liver microsomes, *Arch Pharm Res* 26: 631-637.

Lee HB and Blaufox MD (1985) Blood volume in the rat. J Nucl Med 26:72-76.

Liu J, Cao R, Xu M, Wang X, Zhang H, Hu H, Li Y, Hu Z, Zhang W, and Wang M (2020) Hydroxychloroquine, a less toxic derivative of chloroquine, is effective in inhibiting SARS-CoV-2 infection in vitro, *Cell Discovery* 6:16.

Lullman H and Wehling M (1979) The binding of drugs to different polar lipids in vitro, *Biochem Pharmacol* 28: 3409-3415.

MacIntyre AC and Cutler DJ (1988) Role of lysosomes in hepatic accumulation of chloroquine, *J Pharm Sci* 77: 196-199.

MacIntyre AC and Cutler DJ (1993) Kinetics of chloroquine uptake into isolated rat hepatocytes, *J Pharm Sci* 82: 592-600.

McChesny EW, Banks WF, and Sullivan DJ (1965) Metabolism of chloroquine and hydroxychloroquine in albino and pigmented rats, *Toxicol Appl Pharmacol* 7: 627-636.

McChesney EW, Conway WD, Banks WF, Rogers JE, Shekosky JM, Grace AJ, Jensen AF and Sullivan DJ (1966) Studies of the metabolism of some compounds of the 4-amino-7-chloroquinoline series. *J Pharmacol Exp Ther* 151:482-493.

McChesny EQ, Banks WF, and Fabian RJ (1967) Tissue distribution of chloroquine, hydroxychloroquine, and desethylchloroquine in the rat, Toxicol Appl Pharmacol 10: 501-513.

Moore BR, Page-Sharp M, Stoney JR, Bett KF, Jago JD, and Batty KT (2011) Pharmacokinetics, pharmacodynamics, and allometric scaling of chloroquine in a murine malaria model, *Antimicrob Ag Chemother* 55: 3899 – 3907.

Myers BM, Tietz PS, Tarara JE, and LaRusso NF (1995) Dynamic measurements of the acute and chronic effects of lysosomotropic agents on hepatocyte lysosomal pH using flow cytometry, *Hepatology* 22: 1519-1526.

Olatunde IA (1971) Chloroquine concentrations in the skin of rabbits and man. *Br J Pharmacol* 43:335-340.

Osifo NG (1980) Chloroquine pharmacokinetics in tissues of pyrogen treated rats and implications for chloroquine related pruritus, *Res Commun Chem Path Pharmacol* 30: 419-430.

Plantone D and Koudriavtseva T (2018) Current and future use of chloroquine and hydroxychloroquine in infectious, immune, neoplastic, and neurological diseases: A mini-review. Clin Drug Investig. 38:653-671.

Poulin P and Theil FP (2002) Prediction of pharmacokinetics prior to in vivo studies. 1. Mechanism-based prediction of volume of distribution. *J Pharm Sci* 91:129-156.

Qaseem A, Yost J, Etxeandia-Ikobaltzeta I, et al, on behalf of the Scientific Medical Policy Committee of the American College of Physicians (2020) Should clinicians use chloroquine or hydroxychloroquine alone or in combination with azithromycin for the prophylaxis or treatment of COVID-19? Living practice points from the American College of Physicians (Version 1), Ann Intern Med 173: 137-143.

Rodgers T, Leahy D, and Rowland M (2005) Physiologically based pharmacokinetic modeling 1: Predicting the tissue distribution of moderate-to-strong bases, *J Pharm Sci* 94: `259-276.

Rodgers T and Rowland M (2006) Physiologically based pharmacokinetic modelling 2: Predicting the tissue distribution of acids, very weak bases, neutrals and zwitterions. *J Pharm Sci* 95:1238-1257.

Rodionov N, Graph Digitizer, Version 1.9.2000 (http://geocities.com/graph digitizer/).

Savarino A, Boelaert JR, Cassone A, Majori G, and Cauda R (2003) Effects of chloroquine on viral infections: An old drug against today's diseases? *The Lancet Infectious Diseases* 3: 722-727.

Sawada Y, Hanano M, Sugiyama Y, Harashima H and Iga T (1984) Prediction of the volumes of distribution of basic drugs in humans based on data from animals. *J Pharmacokinet Biopharm* 12:587-596.

Schrezenmeier E and Dorner T (2020), Mechanisms of action of hydroxychloroquine and chloroquine: Implications for rheumatology, *Nature Reviews Rheumatology* 16: 155-166.

Schmitt MV, Lienau P, Fricker G, and Reichel A (2019), Quantitation of lysosomal trapping of basic lipophilic compounds using in vitro assays and in silico predictions based on the determination of the full pH profile of the endo-/lysosomal system in rat hepatocytes, *Drug Met Dispos* 47: 49-57.

Schroeder RL and Gerber JP (2014) Chloroquine and hydroxychloroquine binding to melanin: Some possible consequences for pathologies, *Toxicol Rep* 1: 963-968.

Shi TT, Yu XX, Yan LJ, and Xiao HT (2017) Research progress of hydroxychloroquine and autophagy inhibitors on cancer, *Cancer Chemother Pharmacol* 79:287-294.

29

Tett SE, Cutler DJ, Day RO, and Brown KF (1988) A dose-ranging study of the pharmacokinetics of hydroxychloroquine following intravenous administration to healthy volunteers, *Br J Clin Pharmacol* 26, 303-313.

Tietz PS, Yamazaki K, and LaRusso NF (1990) Time-dependent effects of chloroquine on pH of hepatocyte lysosomes, *Biochem Pharmacol* 40: 1419-1421.

Trapp S, Rosania GR, Horobin RW and Kornhuber J (2008) Quantitative modeling of selective lysosomal targeting for drug design. *Eur Biophys J* 37:1317-1328.

Walker O, Birkett DJ, Alvan G, Gustafsson LL, and Sjoqvist F, (1983) Characterization of chloroquine plasma protein binding in man, *Br J Clin Pharmac* 15: 375-377.

Watanabi and Kozaki A (1978) Relationship between partition coefficient and apparent volumes of distribution for basic drugs. I, *Chem Pharm Bull* 26: 665-667.

White NJ, (1985) Clinical pharmacokinetics of antimalarial drugs. *Clin Pharmacokinet* 10, 187–215.

Yokogawa K, Ishizki J, Ohkuma S, and Miyamoto K, (2002) Influence of lipophilicity and lysosomal accumulation in tissue distribution kinetics of basic drugs: A physiologically based pharmacokinetic model, *Methods Find Exp Clin Pharmacol* 24: 81-93.

Yu DY, Alder VA and Cringle SJ (1991) Measurement of blood flow in rat eyes by hydrogen clearance. *Am J Physiol* 261:H960-968.

Zheng N, Zhang X, and Rosania GR (2011) Effect of phospholipidosis on the cellular pharmacokinetics of chloroquine, *J Pharmacol Exp Ther* 336: 661-67.

Footnotes

This work was supported by NIH Grant R35 GM131800.

No author has an actual or perceived conflict of interest with the contents of this article.

This article has Supplemental Materials available at jpet.aspetjournals.org.

Legends to Figures

Figure 1. Schematic of the PBPK model structure for chloroquine. Parameters and symbols are defined in the text and tables. Lines with arrows indicate plasma flows and drug transport and elimination.

Figure 2. Schematic of lysosomal distribution model structure for chloroquine. Parameters and symbols are defined in the text and tables. Lines with arrows indicate plasma flows and drug transfer. The lysosome model was applied to all tissues except eye and remainder.

Figure 3. Chloroquine concentration-time profiles for all tissues after 10 mg/kg IP single-dosing in rats. Measured chloroquine concentrations in plasma, red blood cells (RBC) and tissues are indicated by different symbols and black solid lines show the PBPK model fitting. Data are from (Adelusi and Salako, 1982a).

Figure 4. Model-predicted lysosome, cytosol, interstitial space (IS), neutral lipid (NL), neutral phospholipid (NP), and acidic phospholipid (AP) chloroquine concentrations versus time after 10 mg/kg IP dosing in rats. Solid symbols are observed values and black lines are PBPK-fitted total tissue concentrations.

Figure 5. Model-predicted lysosome pH values versus time in indicated tissues after 10 mg/kg IP dosing in rats. Broken line indicates the expected initial rise caused by influx of drug, and dot-dash line indicates the presumed lysosomal baseline and steady-state pH.

Figure 6. Plasma concentration-time profiles of chloroquine after single oral dosing in healthy humans. Black lines show the PBPK model fitting. Data were digitized from (Frisk-Holmberg et al, 1984).

Figure 7. Model-predicted lysosome, cytosol, interstitial space (IS), neutral lipid (NL), neutral phospholipid (NP), and acidic phospholipids (AP) chloroquine concentrations versus time in four indicated tissues after 600 mg oral dosing in man.

Table 1. Physiological parameters of tissues for chloroquine in rat and man

Tissue	Volume (V, mL/kg)		Plasma Flow (Q, mL/h/kg)		Fractional Interstitial Space (%) [d]
	Rat [a, b]	Man [b]	Rat [b]	Man [b]	
Liver	32.3	25.7	2191	628.6	16.1
Kidney	5.25	4.45	1385	484.6	27.3
Lung	2.64	7.60	11181 [c]	2769	33.6
Spleen	0.973	2.60	679	138.6	20.7
Heart	2.19	4.71	574	110.7	32.0
Brain	4.64	20.1	248	315.7	16.2
Muscle	422.7	400	3512	528.9	11.8
Skin	174.5	37.1	758	160.6	38.2
Eye	0.74 [c]	0.214 [c]	99.6 [c]	0.073 [c]	-
Blood	105.3	79.1	18641	4615	-
Plasma Artery	21.1	13.7	11185 [c]	2769 [c]	-
Plasma Vein	42.1	32.1	11185 [c]	2769 [c]	-
Remainder	290.9	452.1	1735	401	-
GFR (mL/h/kg) [e] Rat			315		
GFR (mL/h/kg) [e] Man			111		

[a] Corrected for residual blood volume (Bernareggi and Rowland, 1991)

[b] From (Brown et al, 1997)

[c] From (Feke et al, 1989), (Yu et al, 1991), and (Geng et al, 2009)

[d] From (Rodgers et al, 2005)

[e] From (Davies B and Morris T et al, 1993)

Table 2. Summary of fitted and observed chloroquine pharmacokinetic parameters for rat (CV%)

Tissue	B_{max} (µg/mL)	K_D (µg/mL)	PS (mL/h/kg)	C_{tissue}/C_{plasma}			Estimated Kp [a] by GastroPlus™			
				10 h	50 h	150 h	Method 1	Method 2	Method 3	Method 4
Liver	36.8 (71.9)	K_{D1}: 0.00452 (17.7)	PS_1:7297 (43.2)	150	318	634	7.10	10.0	376	858
Kidney	14.2 (12.3)	K_{D1}: 0.00452 (17.7)	PS_2:269 (18.6)	81.8	182	421	4.26	5.04	403	750
Lung	15.6 (9.31)	K_{D1}: 0.00452 (17.7)	PS_2:269 (18.6)	129	275	625	8.44	14.7	319	597
Spleen	12.9 (8.58)	K_{D1}: 0.00452 (17.7)	PS_2:269 (18.6)	131	267	589	4.34	5.16	255	403
Heart	3.78 (8.68)	K_{D1}: 0.00452 (17.7)	PS_3:148 (29.9)	32.4	65.6	143	4.75	5.73	181	261
Brain	1.74 (8.89)	K_{D1}: 0.00452 (17.7)	PS_3:148 (29.9)	19.0	38.4	84.5	11.3	16.1	35.6	40.2
Muscle	0.525 (10.9)	K_{D2}: 0.00544 (21.8)	PS_4: 3798 (35.2)	6.32	12.0	23.9	4.33	6.14	124	165
Skin	0.695 (10.6)	K_{D2}: 0.00544 (21.8)	PS_4: 3798 (35.2)	5.77	10.9	21.4	5.29	7.50	107	139
Eye	1.49 (9.55)	K_{D2}: 0.00544 (21.8)	-	19.4	35.6	74.5	NA	NA	NA	NA
Remainder	7.04 (30.8)	K_{D1}: 0.00452 (17.7)	-		-	-	NA	NA	NA	NA

K_b	RBC to plasma partition coefficient of RBC	11.6 (10.8)
ka_{liver}	Absorption rate constant into liver (h^{-1})	0.0306 (9.40)
ka_{plasma}	Absorption rate constant into plasma (h^{-1})	0.372 (20.6)
$CL_{u,int}$	Hepatic intrinsic clearance (mL/h/kg)	11600 (70.3)
$CL_{s,renal}$	Systemic renal clearance (mL/h/kg)	630 [b]
fu	Free fraction of drug in plasma (%)	40.0 [c]

[a] Estimated partition coefficient (Kp) value using GastroPlus: Method 1, (Poulin and Theil, 2002); 2, (Berezhkovskiy, 2004); 3, (Rodgers and Rowland, 2006); 4, (SimulationsPlus).

[b] Fixed to 2-fold GFR

[c] From (Ducharme and Farinotti, 1996)

Table 3. Summary of parameters for lysosome distribution model

Tissue	Lysosome volume (%) [a]	Component fraction (%) [b]									
		Interstitial Space	Cytosol		Neutral Lipid		Neutral Phospholipid		AP (mg/g) [c]	
			Rat	*Man*	*Rat*	*Man*	*Rat*	*Man*	*Rat*	*Man*
Liver	9.55	16.1	57.3	59.0	1.40	3.48	2.40	2.52	4.56	4.56
Kidney	3.28	27.3	48.3	51.0	1.20	2.07	2.42	1.62	5.03	5.03
Lung	2.77	33.6	44.6	47.5	2.20	0.30	1.28	0.80	3.91	3.91
Spleen	3.18	20.7	57.9	58.1	0.77	0.20	1.13	1.98	3.18	3.18
Heart	0.595	32.0	45.6	45.0	1.40	1.15	1.11	1.66	2.25	2.25
Brain	0.481	16.2	62.0	60.8	3.90	5.10	0.15	5.65	0.40	9.60
Muscle	0.126	11.8	63.0	64.2	1.00	2.38	0.72	0.72	1.53	1.53
Skin	0.096	38.2	29.1	33.6	6.00	2.84	0.44	1.11	3.18	3.18
RBC	-	-	60.3		0.17		0.29		0.50	
pKa1					10.1					
pKa2					8.40					
LogP					4.63					
pH [d]	Lysosome				5.0 (at 10 h)					
	Cytosol				7.0					
	IS and Plasma				7.4					
Fn	Lysosome				3.16E-09 (at 10 h)					
	Cytosol				3.04E-05					
	IS and Plasma				1.81E-04					

[a] Calculated based on 10 h fitted data

[b] From (Rodgers et al, 2005) and (Poulin and Theil, 2002).

[c] AP (acidic phospholipid concentration)

[d] From (Assmus et al, 2017)

Table 4. Summary of assigned and fitted chloroquine pharmacokinetic parameters for man

(CV%)

Parameter	Description	Estimated value
$CL_{u,int}$	Hepatic clearance (mL/h/kg)	1060 (14.5)
ka_{oral}	Absorption rate constant (h^{-1})	0.0245 (13.2)
K_{D1}	Dissociation constant (µg/ml)	0.0228 (8.5)
R	Adjustment factor for Kp	7.0 [a]
F	Bioavailability (%)	100 [b]
fu	Free fraction of drug in plasma (%)	40.0 [c]

[a] Based on multiplying PBPK Kp_{tissue} values by the ratio of man-to-rat V_{ss}.

[b] From (Frisk-Holmberg et al, 1984)

[c] From (Ducharme and Farinotti, 1996)
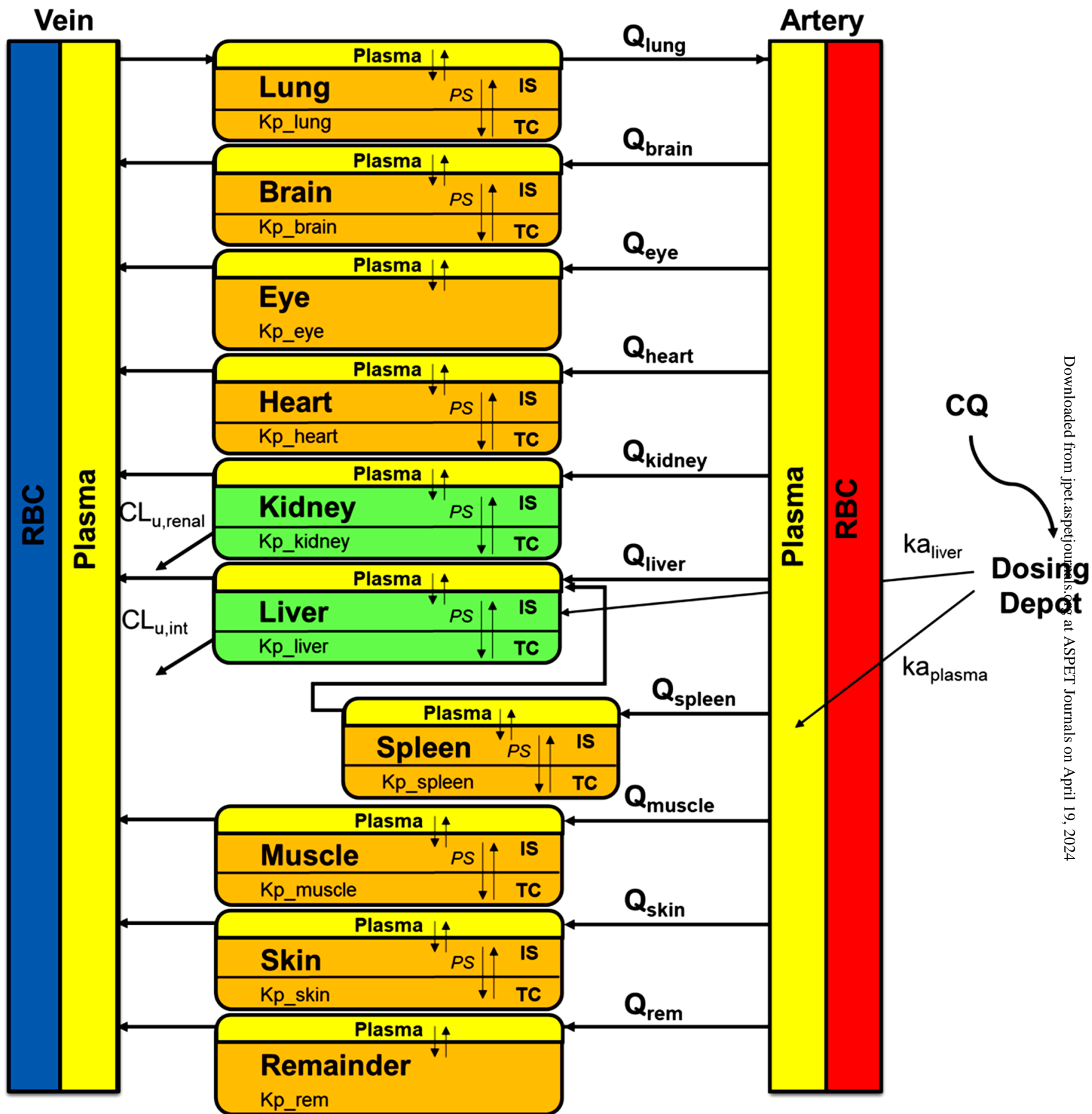
Figure 1
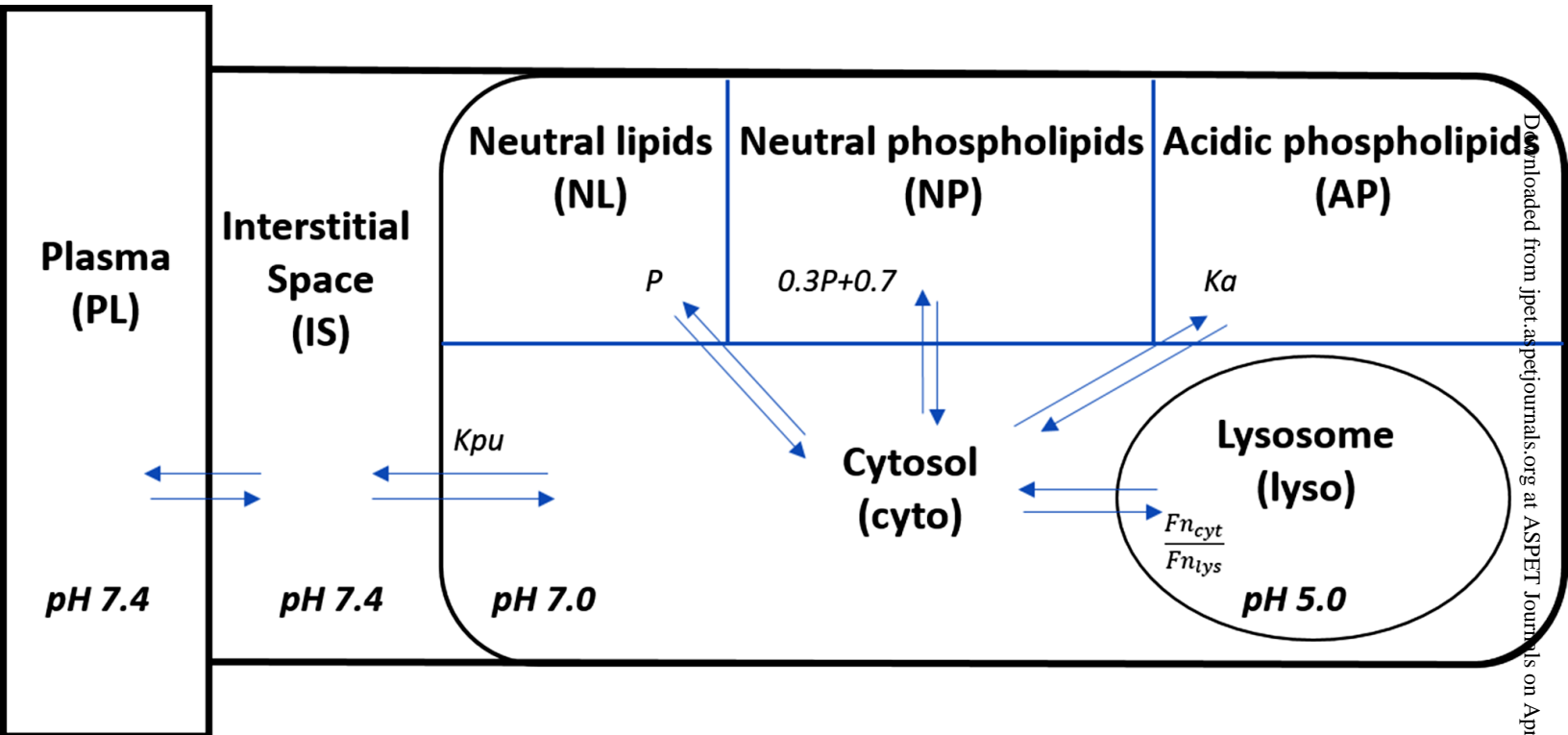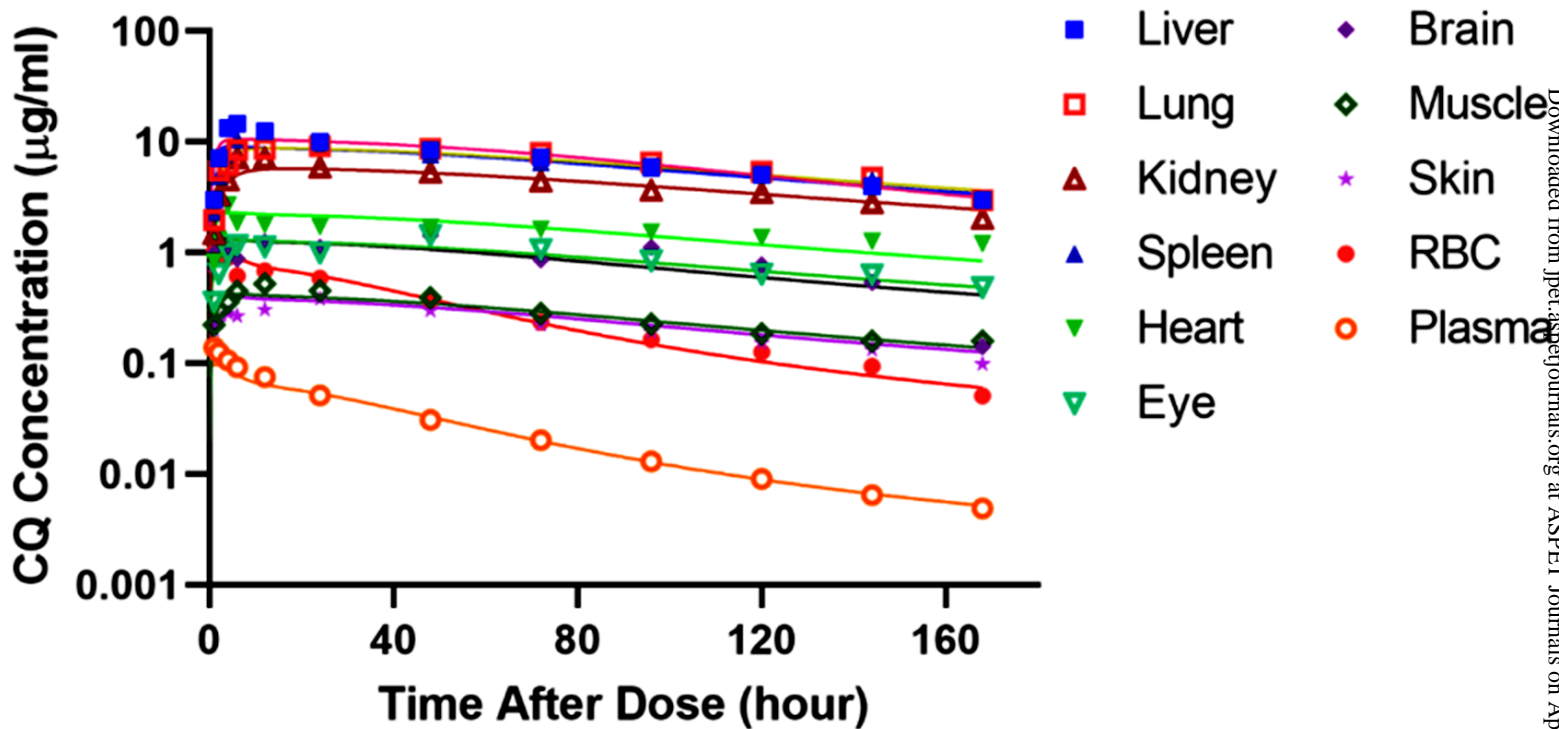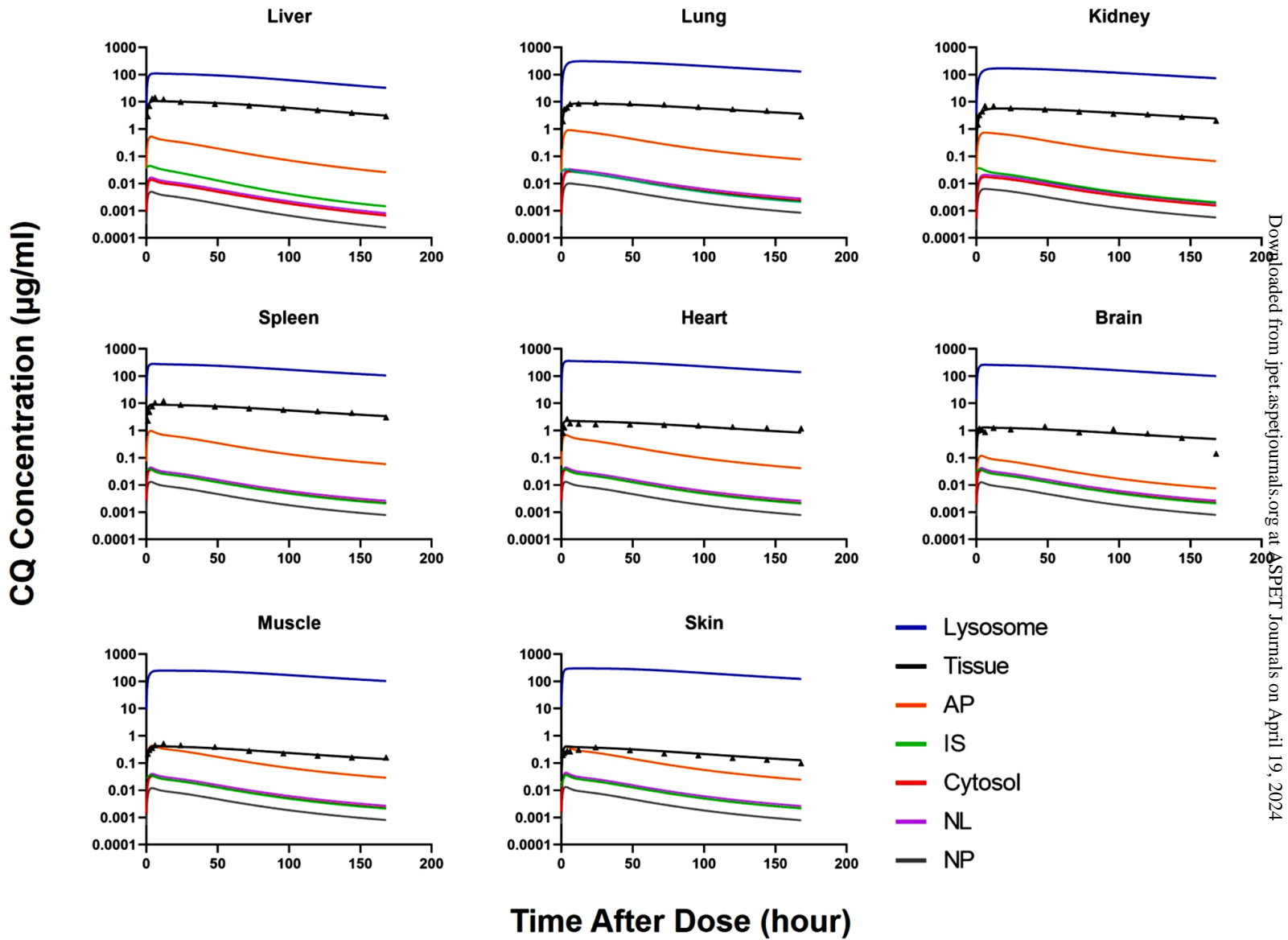
Figure 2

Figure 3

Figure 4
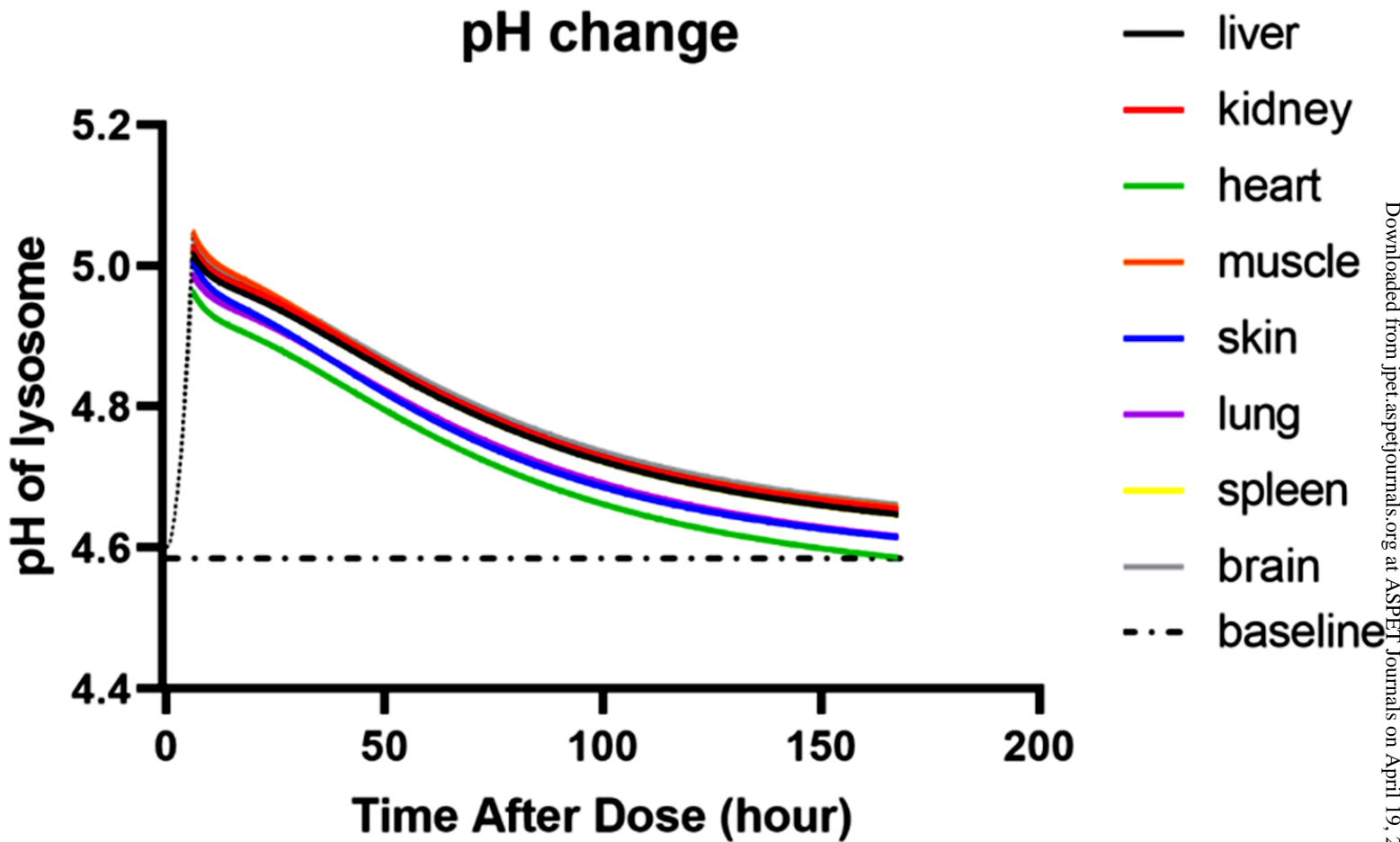
Figure 5
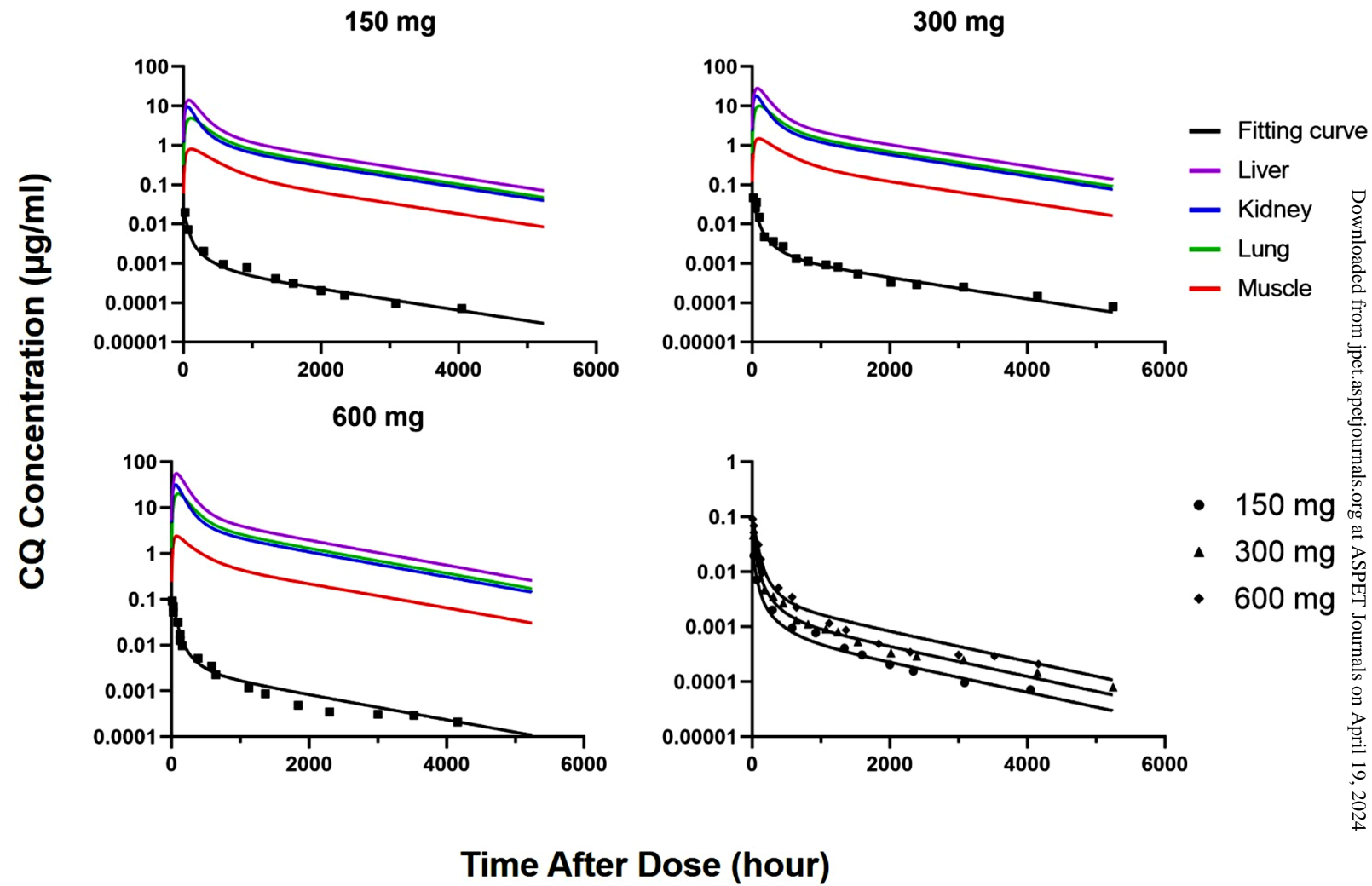
Figure 6
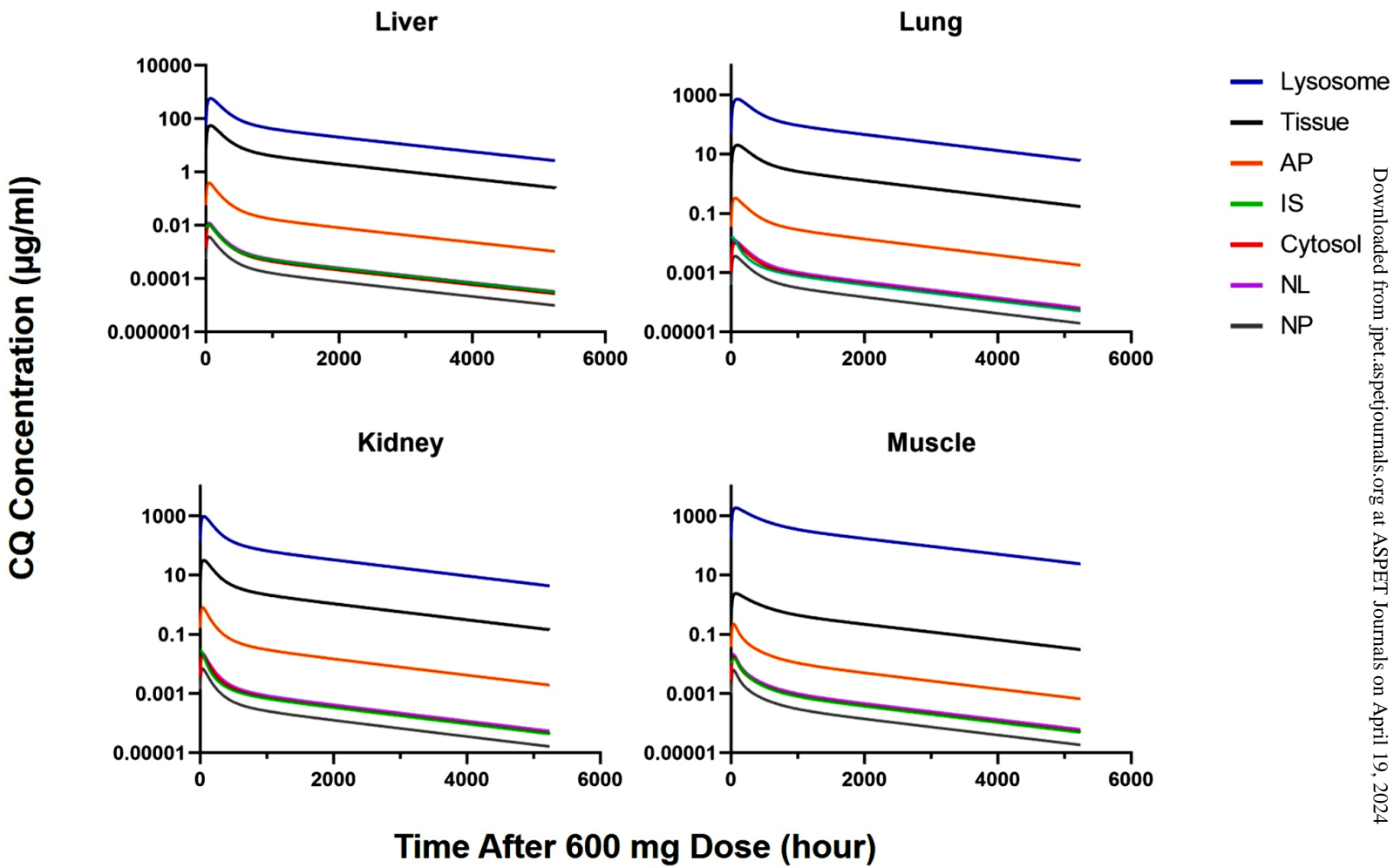
Figure 7

SUPPLEMENTAL MATERIALS

Article title: Physiologically-Based Pharmacokinetics of Lysosomotropic Chloroquine in Rat and Man
Authors: Xin Liu and William J. Jusko
Journal title: Journal of Pharmacology and Experimental Therapeutics
Manuscript number: JPET-AR-2020-000385

Table S1. Comparison of chloroquine pharmacokinetic parameters (Adelusi & Salako, 1982a)

Tissue	T_{max} (h)		C_{max} (µg/mL)		$T_{1/2}$ (h)		β Slope (h^{-1})	
	Original article	PBPK fitting	Original article	PBPK fitting	Original article	PBPK fitting	Original article	PBPK fitting
Liver	7.70	6.00	14.8	10.7	81.7	75.7	0.0085	0.0092
Kidney	10.0	15.5	6.80	5.76	94.1	105	0.0073	0.0066
Lung	22.0	14.3	7.90	8.77	138	97.3	0.0050	0.0071
Spleen	10.0	4.73	9.90	9.12	75.1	80.6	0.0092	0.0086
Heart	16.0	4.73	2.40	2.29	100	79.9	0.0069	0.0087
Muscle	16.0	6.34	0.60	0.424	97.0	71.1	0.0072	0.0098
Skin	24.7	4.06	0.45	0.407	110	67.9	0.0063	0.0102
RBC	1.30	1.69	1.10	1.12	40.0	31.0	0.0170	0.0223
Plasma	1.00	1.69	0.143	0.0969	28.2	31.0	0.0260	0.0223

Table S2. Digitized and recalculated chloroquine plasma and tissue concentration data for rat

Time (h)	Chloroquine Concentration (µg/mL)										
	Liver	Kidney	Lung	Spleen	Heart	Brain	Muscle	Skin	Eye	RBC	Plasma
1	2.992	1.480	1.959	2.322	0.832	0.997	0.223	0.198	0.361	1.012	0.139
2	7.095	3.305	5.496	4.882	1.310	1.202	0.304	0.237	0.650	0.976	0.125
4	13.35	4.478	6.193	7.777	2.694	1.070	0.358	0.284	0.982	0.907	0.107
6	14.64	7.143	8.486	10.58	1.857	0.882	0.449	0.266	1.175	0.615	0.092
12	12.55	7.097	8.646	12.28	1.778	1.253	0.523	0.307	1.137	0.685	0.075
24	10.09	5.857	9.096	8.955	1.718	1.116	0.453	0.381	1.004	0.587	0.051
48	8.459	5.306	8.734	7.665	1.689	1.437	0.393	0.299	1.453	0.375	0.031
72	7.254	4.391	7.962	6.533	1.618	0.864	0.283	0.226	1.076	0.236	0.020
96	5.954	3.648	6.532	5.816	1.530	1.122	0.227	0.194	0.858	0.163	0.013
120	5.012	3.468	5.387	5.145	1.371	0.778	0.185	0.154	0.644	0.127	0.009
144	3.980	2.815	4.765	4.514	1.261	0.540	0.160	0.133	0.636	0.094	0.006
168	2.978	2.028	2.970	3.079	1.209	0.142	0.160	0.098	0.489	0.051	0.005

From: (Adelusi & Salako, 1982a)

Table S3. Digitized plasma chloroquine concentrations in man.

150 mg		300 mg		600 mg	
Time (h)	ng/mL	Time (h)	ng/mL	Time (h)	ng/mL
24	19.74	24	46.51	8	91.32
75	7.177	48	25.69	12	68.83
296	2.031	72	35.24	24	51.89
583	0.948	95	14.77	95	31.30
926	0.778	177	4.720	130	17.02
1342	0.408	308	3.545	144	12.64
1600	0.308	453	2.698	156	9.688
2001	0.205	641	1.315	385	5.132
2345	0.155	815	1.116	581	3.450
3090	0.096	1076	0.913	647	2.258
4050	0.072	1250	0.807	1121	1.164
		1540	0.534	1366	0.866
		2018	0.332	1840	0.487
		2394	0.291	2298	0.347
		3075	0.248	3001	0.310
		4148	0.146	3524	0.292
		5250	0.080	4162	0.210

From (Frisk-Holmberg et al, 1984)

Predictability of the PBPK model for chloroquine in rats for a different data set

A second study of the pharmacokinetics and tissue distribution of chloroquine was carried out by (Adalusi and Salako, 1982b). Groups of Wistar rats were fed with different diets including (commercial rat diet, cassava-based diet [altered carbohydrate source], and kwashiorkorigenic diet [low protein]) to assess effects of malnourishment. The data from the first group were not graphed, so data from the cassava-based diet group were digitized as this group showed similar body weights as the control group. Chloroquine was given intraperitoneally at a dose of 10 mg/kg. Blood and tissues were taken at various times. Graphical data were digitized to yield the numerical values listed in Table S4.

Table S4. Plasma and tissue concentrations of chloroquine

Time (hour)	Chloroquine concentrations (µg/mL)			
	Plasma	RBC	Liver	Skin
1	0.1297	1.076	5.19	0.212
2	0.1148	1.003	6.40	0.233
4	0.1023	0.907	11.88	0.256
6	0.0924	0.821	13.72	0.288
12	0.0768	0.737	12.55	0.298
24	0.0536	0.628	10.94	0.401
48	0.0316	0.369	7.30	0.403
72	0.0201	0.244	5.72	0.332
96	0.0126	0.147	4.94	0.259
120	0.0098	0.100	4.51	0.199
144	0.0068	0.087	3.77	0.169
168	0.0054	0.071	3.20	0.140

The first-stage PBPK model and parameters obtained from the main study were used to simulate the available tissue and plasma profiles from this study. The figure below demonstrates excellent capture of the liver, RBC, skin, and plasma profiles from this study.
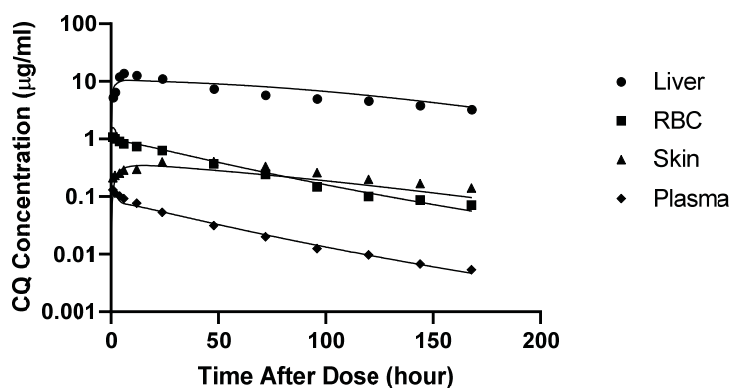
Figure S1. Simulation for rat tissues, RBC and plasma concentrations with PBPK model

Adapt code for rat PBPK model

```
1 c*******************************************************************************
  *************************************************
2 C ADAPT *
3 C Version 5 *
4 C***************************************************************************
5 C *
6 C MODEL *
7 C *
8 C This file contains Fortran subroutines into which the user *
9 C must enter the relevant model equations and constants. *
10 C Consult the User's Guide for details concerning the format for *
11 C entered equations and definition of symbols. *
12 C *
13 C 1. Symbol- Parameter symbols and model constants *
14 C 2. DiffEq- System differential equations *
15 C 3. Output- System output equations *
16 C 4. Varmod- Error variance model equations *
17 C 5. Covmod- Covariate model equations (ITS,MLEM) *
18 C 6. Popinit- Population parameter initial values (ITS,MLEM) *
19 C 7. Prior - Parameter mean and covariance values (ID,NPD,STS) *
20 C 8. Sparam- Secondary parameters *
21 C 9. Amat - System state matrix *
22 C *
23 C***************************************************************************
24 C#################################################################C
25 Subroutine SYMBOL
26 Implicit None
27 Include 'globals.inc'
28 Include 'model.inc'
29 CC
30 C-----------------------------------------------------------------C
31 C Enter as Indicated C
32 C----c------------------------------------------------------------C
33 NDEqs = 22 ! Enter # of Diff. Eqs.
34 NSParam = 21 ! Enter # of System Parameters.
35 NVparam = 2 ! Enter # of Variance Parameters.
36 NSecPar = 0 ! Enter # of Secondary Parameters.
37 NSecOut = 0 ! Enter # of Secondary Outputs (not used).
38 Ieqsol = 1 ! Model type: 1 - DIFFEQ, 2 - AMAT, 3 - OUTPUT only.
39 Descr = ' simple PBPK of QC '
40 CC
41 C-----------------------------------------------------------------C
42 C Enter Symbol for Each System Parameter (eg. Psym(1)='Kel') C
43 C----c------------------------------------------------------------C
44 Psym(1)='Bmax_liver'
45 Psym(2)='Bmax_kidney'
46 Psym(3)='Bmax_heart'
47 Psym(4)='Bmax_muscle'
48 Psym(5)='Bmax_skin'
49 Psym(6)='Bmax_lung'
50 Psym(7)='Bmax_spleen'
```

```fortran
51 Psym(8)='Bmax_brain'
52 Psym(9)='Bmax_eye'
53 Psym(10)='Bmax_carcass'
54 Psym(11)='KD'
55 Psym(12)='KD2'
56 Psym(13)='kap'
57 Psym(14)='Kal'
58 Psym(15)='CL_u,int'
59 Psym(16)='CL_u,renal'
60 Psym(17)='ft'
61 Psym(18)='PS'
62 Psym(19)='PS2'
63 Psym(20)='PS3'
64 Psym(21)='PS4'
65 CC
66 C------------------------------------------------------------------C
67 C Enter Symbol for Each Variance Parameter {eg: PVsym(1)='Sigma'} C
68 C----c------------------------------------------------------------C
69 PVsym(1)='sigma'
70 PVsym(2)='intercept'
71 CC
72 C------------------------------------------------------------------C
73 C Enter Symbol for Each Secondary Parameter {eg: PSsym(1)='CLt'} C
74 C----c------------------------------------------------------------C
75 C------------------------------------------------------------------C
76 C------------------------------------------------------------------C
77 C
78 Return
79 End
80 C#####################################################################C
81 Subroutine DIFFEQ(T,X,XP)
82 Implicit None
83 Include 'globals.inc'
84 Include 'model.inc'
85 Real*8 T,X(MaxNDE),XP(MaxNDE)
86 Real*8 ka, F, Cl_kidney, Cl_liver, fu
87 Real*8 Bmax_liver, Kp_liver ,Kp_heart,KD3
88 Real*8 Kp_kidney, Bmax_kidney, Bmax_muscle,Kp_carcass
89 Real*8 Bmax_heart, Kp_muscle, Kp_skin, Bmax_skin,KD,KD2
90 Real*8 Q_liver, Q_heart, Q_gut, Q_kidney, Q_skin,Q_muscle
91 Real*8 Q_slow,Q_rapid, Q_blood,Q_carcass,ft_s,kal
92 Real*8 V_liver,V_kidney, V_muscle,V_blood,V_carcass,V_plasma
93 Real*8 V_heart,V_slow, V_rapid, V_skin, V_gut,Cl,ft_m
94 Real*8 Vmaxr,Kmr, Vmaxl,Kml,ft_h,ft_k,ft_l,fi,GFR,ft_c
95 Real*8 Q_lung, Q_spleen, Q_brain, Q_eye, Kp_lung, Kp_spleen
96 Real*8 Kp_brain, Kp_eye, V_lung,V_spleen, V_brain, V_eye
97 Real*8 V_artery, V_vein,Bmax_spleen,ft_b,ft_e,PS,PS2,PS3,PS4
98 Real*8 Bmax_lung,Bmax_eye,Bmax_brain,Bmax_carcass
99 Real*8 V_liver2,V_kidney2,V_heart2,V_muscle2,V_skin2,V_lung2
100 real*8 V_spleen2,V_brain2
101 CC
102 C------------------------------------------------------------------C
103 C Enter Differential Equations Below {e.g. XP(1) = -P(1)*X(1) } C
```

```
104 C----c--------------------------------------------------------------C
105 Bmax_liver=P(1)
106 Bmax_kidney=P(2)
107 Bmax_heart=P(3)
108 Bmax_muscle=P(4)
109 Bmax_skin=P(5)
110 Bmax_lung=P(6)
111 Bmax_spleen=P(7)
112 Bmax_brain=P(8)
113 Bmax_eye=P(9)
114 Bmax_carcass=P(10)
115 KD=P(11)
116 KD2=P(12)
117 ka=P(13)
118 kal=P(14)
119 Cl=P(15)
120 Cl_kidney=P(16)
121 ft_e=1.0
122 ft_k=1.0
123 ft_l=1.0
124 ft_m=P(17)
125 ft_h=1.0
126 ft_b=1.0
127 ft_s=P(17)
128 ft_c=1.0
129 PS=P(18)
130 PS2=P(19)
131 PS3=P(20)
132 PS4=P(21)
133 ! Tissue volume (mL/kg)
134 V_kidney=5.25*0.273
135 V_liver=32.31*0.161
136 V_heart=2.19*0.320
137 V_skin=174.45*0.382
138 V_muscle=422.68*0.118
139 V_lung=2.642*0.336
140 V_spleen=0.973*0.207
141 V_brain=4.643*0.162
142 V_eye=0.74
143 V_artery= 21.1
144 V_vein=42.1
145 V_carcass=290.92
146 V_kidney2=5.25*(1.0-0.273)
147 V_liver2=32.31*(1.0-0.161)
148 V_heart2=2.19*(1.0-0.32)
149 V_skin2=174.45*(1.0-0.382)
150 V_muscle2=422.68*(1.0-0.118)
151 V_lung2=2.642*(1.0-0.336)
152 V_spleen2=0.973*(1.0-0.207)
153 V_brain2=4.643*(1.0-0.162)
154 ! plasma flow was used to describe the flow rate to each tissues (mL/h/kg)
155 Q_kidney=1385
156 Q_liver= 2191
```

```
157 Q_heart= 574
158 Q_skin= 758
159 Q_muscle= 3512
160 Q_carcass=1735
161 Q_lung =11181.6
162 Q_spleen=679
163 Q_brain=248
164 Q_eye=99.6
165 GFR=315
166 !Kp
167 fu=0.4
168 Kp_heart=1+Bmax_heart/(KD+X(5))
169 Kp_kidney=1+Bmax_kidney/(KD+X(4))
170 Kp_liver=1+Bmax_liver/(KD+X(3))
171 Kp_muscle=1+Bmax_muscle/(KD2+X(7))
172 Kp_skin=1+Bmax_skin/(KD2+X(6))
173 Kp_lung=1+Bmax_lung/(KD+X(8))
174 Kp_spleen=1+Bmax_spleen/(KD+X(9))
175 Kp_brain=1+Bmax_brain/(KD+X(10))
176 Kp_eye=fu*(1+Bmax_eye/(KD2+fu*X(1)))
177 Kp_carcass=fu*(1+Bmax_carcass/(KD+fu*X(1)))
178 !IP bolus in rat
179 !artery
180 XP(1)=(Q_lung*X(8)/fu+ka*X(2)-fu*GFR*X(1)
181   -(Q_liver+Q_kidney+Q_heart+Q_skin*ft_s+
182   Q_muscle*ft_m+Q_spleen+Q_brain+Q_eye*ft_e+
183   Q_carcass*ft_c)*X(1))/V_artery
184 !vein
185 XP(14)=((Q_liver+Q_spleen)*X(3)/fu+Q_kidney*X(4)/fu+Q_heart*
186   X(5)/fu+Q_skin*ft_s*X(6)/fu+Q_muscle*ft_m*X(7)/fu
187   +Q_brain*ft_b*X(10)/fu+Q_eye*ft_e*X(11)/
188   Kp_eye+
189   Q_carcass*ft_c*X(12)/Kp_carcass-Q_lung*X(14))/V_vein
190 !absorption in plasma
191 XP(2)=-ka*X(2)
192 !absorption in liver
193 XP(13)=-kal*X(13)
194 !liver
195 XP(3)=(Q_liver*(X(1)-X(3)/fu)+Q_spleen*(X(9)/fu-X(3)/fu)
196   +kal*X(13)-PS*(X(3)-
197   X(15)/Kp_liver))/V_liver
198 XP(15)=(PS*(X(3)-X(15)/Kp_liver)-
199   Cl*X(15)/Kp_liver)/V_liver2
200 !kidney
201 XP(4)=(Q_kidney*(X(1)-X(4)/fu)-PS2*(X(4)-
202   X(16)/Kp_kidney))/V_kidney
203 XP(16)=(PS2*(X(4)-X(16)/Kp_kidney)-
204   Cl_kidney*X(16)/Kp_kidney)/V_kidney2
205 !heart
206 XP(5)=(Q_heart*(X(1)-X(5)/fu)-PS3*(X(5)-
207   X(17)/Kp_heart))/V_heart
208 XP(17)=PS3*(X(5)-X(17)/Kp_heart)/V_heart2
209 !skin
```

```fortran
210 XP(6)=(Q_skin*ft_s*(X(1)-X(6)/fu)-PS4*(X(6)-
211   X(18)/Kp_skin))/V_skin
212 XP(18)=PS4*(X(6)-X(18)/Kp_skin)/V_skin2
213 !muscle
214 XP(7)=(Q_muscle*ft_m*(X(1)-X(7)/fu)-PS4*(X(7)-
215   X(19)/Kp_muscle))/V_muscle
216 XP(19)=PS4*(X(7)-X(19)/Kp_muscle)/V_muscle2
217 !lung
218 XP(8)=(Q_lung*(X(14)-X(8)/fu)-PS2*(X(8)-
219   X(20)/Kp_lung))/V_lung
220 XP(20)=PS2*(X(8)-X(20)/Kp_lung)/V_lung2
221 !spleen
222 XP(9)=(Q_spleen*(X(1)-X(9)/fu)-PS2*(X(9)-
223   X(21)/Kp_spleen))/V_spleen
224 XP(21)=PS2*(X(9)-X(21)/Kp_spleen)/V_spleen2
225 !brain
226 XP(10)=(Q_brain*(X(1)-X(10)/fu)-PS3*(X(10)-
227   X(22)/Kp_brain))/V_brain
228 XP(22)=PS3*(X(10)-X(22)/Kp_brain)/V_brain2
229 !eye
230 XP(11)=Q_eye*ft_e*(X(1)-X(11)/Kp_eye)/V_eye
231 !carcass
232 XP(12)=Q_carcass*ft_c*(X(1)-X(12)/Kp_carcass)/V_carcass
233 C----------------------------------------------------------------C
234 C----------------------------------------------------------------C
235 C
236 Return
237 End
238 C##############################################################################C
239 Subroutine OUTPUT(Y,T,X)
240 Implicit None
241 Include 'globals.inc'
242 Include 'model.inc'
243 Real*8 Y(MaxNOE),T,X(MaxNDE)
244 Real*8 Bmax_liver, Kp_liver ,Kp_heart
245 Real*8 Kp_kidney, Bmax_kidney, Bmax_muscle,Bmax_blood,fu
246 Real*8 Bmax_heart, Kp_muscle, Kp_skin, Bmax_skin,KD
247 Real*8 Q_liver, Q_heart, Q_gut, Q_kidney, Q_skin,Q_muscle
248 Real*8 Q_eye,Q_slow,Q_rapid, Q_blood,Q_carcass,Kp_blood
249 Real*8 V_liver,V_kidney, V_muscle,V_blood,V_carcass,V_plasma
250 Real*8 V_heart,V_slow, V_rapid, V_skin, V_gut,Cl
251 Real*8 Vmaxr,Kmr, Vmaxl,Kml
252 Real*8 Vl_liver,Vl_kidney,Vl_heart,Vl_skin,Vl_muscle,Vl_carcass
253 Real*8 At_liver,At_kidney,At_heart,At_skin,At_muscle,At_carcass
254 Real*8 fnc,fnl,N1,N2,EN1,EN2,Pn,PD1,PD2,D1o,D1i,D2o,D2i
255 Real*8 V_liver2,V_kidney2,V_heart2,V_muscle2,V_skin2,V_lung2
256 real*8 V_spleen2,V_brain2
257 Real*8 V_lung
258 real*8 V_spleen,V_brain
259 CC
260 C----------------------------------------------------------------C
261 C Enter Output Equations Below {e.g. Y(1) = X(1)/P(2) } C
262 C----c-----------------------------------------------------------C
```

```fortran
263 Kp_blood=11.6
264 ! Tissue volume (mL/kg)
265 V_kidney=5.25*0.273
266 V_liver=32.31*0.161
267 V_heart=2.19*0.320
268 V_skin=174.45*0.382
269 V_muscle=422.68*0.118
270 V_lung=2.642*0.336
271 V_spleen=0.973*0.207
272 V_brain=4.643*0.162
273 V_kidney2=5.25*(1.0-0.273)
274 V_liver2=32.31*(1.0-0.161)
275 V_heart2=2.19*(1.0-0.32)
276 V_skin2=174.45*(1.0-0.382)
277 V_muscle2=422.68*(1.0-0.118)
278 V_lung2=2.642*(1.0-0.336)
279 V_spleen2=0.973*(1.0-0.207)
280 V_brain2=4.643*(1.0-0.162)
281 Y(1)=(X(3)*V_liver+X(15)*V_liver2)/(V_liver+V_liver2)
282 Y(2)=(X(4)*V_kidney+X(16)*V_kidney2)/(V_kidney+V_kidney2)
283 Y(3)=(X(5)*V_heart+X(17)*V_heart2)/(V_heart+V_heart2)
284 Y(4)=X(1)*Kp_blood
285 Y(5)=(X(7)*V_muscle+X(19)*V_muscle2)/(V_muscle+V_muscle2)
286 Y(6)=(X(6)*V_skin+X(18)*V_skin2)/(V_skin+V_skin2)
287 Y(7)=X(1)
288 Y(8)=(X(8)*V_lung+X(20)*V_lung2)/(V_lung+V_lung2)
289 Y(9)=(X(9)*V_spleen+X(21)*V_spleen2)/(V_spleen+V_spleen2)
290 Y(10)=(X(10)*V_brain+X(22)*V_brain2)/(V_brain+V_brain2)
291 Y(11)=X(11)
292 C---------------------------------------------------------------C
293 C---------------------------------------------------------------C
294 C
295 Return
296 End
297 C################################################################C
298 Subroutine VARMOD(V,T,X,Y)
299 Implicit None
300 Include 'globals.inc'
301 Include 'model.inc'
302 Real*8 V(MaxNOE),T,X(MaxNDE),Y(MaxNOE)
303 CC
304 C---------------------------------------------------------------C
305 C Enter Variance Model Equations Below C
306 C {e.g. V(1) = (PV(1) + PV(2)*Y(1))**2 } C
307 C----c----------------------------------------------------------C
308 V(1) = (PV(2) + PV(1)*Y(1))**2
309 V(2) = (PV(2) + PV(1)*Y(2))**2
310 V(3) = (PV(2) + PV(1)*Y(3))**2
311 V(4) = (PV(2) + PV(1)*Y(4))**2
312 V(5) = (PV(2) + PV(1)*Y(5))**2
313 V(6) = (PV(2) + PV(1)*Y(6))**2
314 V(7) = (PV(2) + PV(1)*Y(7))**2
315 V(8) = (PV(2) + PV(1)*Y(8))**2
```

```fortran
316 V(9) = (PV(2) + PV(1)*Y(9))**2
317 V(10) = (PV(2) + PV(1)*Y(10))**2
318 V(11) = (PV(2) + PV(1)*Y(11))**2
319 C----------------------------------------------------------------C
320 C----------------------------------------------------------------C
321 C
322 Return
323 End
324 C################################################################C
325 Subroutine COVMOD(Pmean, ICmean, PC)
326 C Defines any covariate model equations (MLEM, ITS)
327 Implicit None
328 Include 'globals.inc'
329 Include 'model.inc'
330 Real*8 PC(MaxNCP)
331 Real*8 Pmean(MaxNSP+MaxNDE), ICmean(MaxNDE)
332 CC
333 C----------------------------------------------------------------C
334 C Enter # of Covariate Parameters C
335 C----c-----------------------------------------------------------C
336 NCparam = 0 ! Enter # of Covariate Parameters.
337 CC
338 C----------------------------------------------------------------C
339 C Enter Symbol for Covariate Params {eg: PCsym(1)='CLRenal'} C
340 C----c-----------------------------------------------------------C
341 CC
342 C----------------------------------------------------------------C
343 C For the Model Params. that Depend on Covariates Enter the Equation C
344 C {e.g. Pmean(1) = PC(1)*R(2) } C
345 C----c-----------------------------------------------------------C
346 C----------------------------------------------------------------C
347 C----------------------------------------------------------------C
348 C
349 Return
350 End
351 C################################################################C
352 Subroutine POPINIT(PmeanI,ICmeanI,PcovI,ICcovI, PCI)
353 C Initial parameter values for population program parameters (ITS, MLEM)
354 Implicit None
355 Include 'globals.inc'
356 Include 'model.inc'
357 Integer I,J
358 Real*8 PmeanI(MaxNSP+MaxNDE), ICmeanI(MaxNDE)
359 Real*8 PcovI(MaxNSP+MaxNDE,MaxNSP+MaxNDE), ICcovI(MaxNDE,MaxNDE)
360 Real*8 PCI(MaxNCP)
361 CC
362 C----------------------------------------------------------------C
363 C Enter Initial Values for Population Means C
364 C { e.g. PmeanI(1) = 10.0 } C
365 C----c-----------------------------------------------------------C
366 CC
367 C----------------------------------------------------------------C
368 C Enter Initial Values for Pop. Covariance Matrix (Lower Triang.) C
```

```fortran
369 C { e.g. PcovI(2,1) = 0.25 } C
370 C----c-----------------------------------------------------------C
371 CC
372 C---------------------------------------------------------------C
373 C Enter Values for Covariate Model Parameters C
374 C { e.g. PCI(1) = 2.0 } C
375 C----c-----------------------------------------------------------C
376 C---------------------------------------------------------------C
377 C---------------------------------------------------------------C
378 C
379 Return
380 End
381 C###############################################################C
382 Subroutine PRIOR(Pmean,Pcov,ICmean,ICcov)
383 C Parameter mean and covariance values for MAP estimation (ID,NPD,STS)
384 Implicit None
385 Include 'globals.inc'
386 Include 'model.inc'
387 Integer I,J
388 Real*8 Pmean(MaxNSP+MaxNDE), ICmean(MaxNDE)
389 Real*8 Pcov(MaxNSP+MaxNDE,MaxNSP+MaxNDE), ICcov(MaxNDE,MaxNDE)
390 CC
391 C---------------------------------------------------------------C
392 C Enter Nonzero Elements of Prior Mean Vector C
393 C { e.g. Pmean(1) = 10.0 } C
394 C----c-----------------------------------------------------------C
395 CC
396 C---------------------------------------------------------------C
397 C Enter Nonzero Elements of Covariance Matrix (Lower Triang.) C
398 C { e.g. Pcov(2,1) = 0.25 } C
399 C----c-----------------------------------------------------------C
400 C---------------------------------------------------------------C
401 C---------------------------------------------------------------C
402 C
403 Return
404 End
405 C###############################################################C
406 Subroutine SPARAM(PS,P,IC)
407 Implicit None
408 Include 'globals.inc'
409 Real*8 PS(MaxNSECP), P(MaxNSP+MaxNDE), IC(MaxNDE)
410 CC
411 C---------------------------------------------------------------C
412 C Enter Equations Defining Secondary Paramters C
413 C { e.g. PS(1) = P(1)*P(2) } C
414 C----c-----------------------------------------------------------C
415 C---------------------------------------------------------------C
416 C---------------------------------------------------------------C
417 C
418 Return
419 End
420 C###############################################################C
421 Subroutine AMAT(A)
```

```fortran
422 Implicit None
423 Include 'globals.inc'
424 Include 'model.inc'
425 Integer I,J
426 Real*8 A(MaxNDE,MaxNDE)
427 DO I=1,Ndeqs
428 Do J=1,Ndeqs
429 A(I,J)=0.0D0
430 End Do
431 End Do
432 CC
433 C----------------------------------------------------------------C
434 C Enter non zero elements of state matrix {e.g. A(1,1) = -P(1) } C
435 C----c-----------------------------------------------------------C
436 C----------------------------------------------------------------C
437 C----------------------------------------------------------------C
438 C
439 Return
440 End
441 C###############################################################C
```

Adapt Code for human PBPK model

```
1 c*******************************************************************************
  **************************************************
2 C ADAPT *
3 C Version 5 *
4 C***************************************************************************
5 C *
6 C MODEL *
7 C *
8 C This file contains Fortran subroutines into which the user *
9 C must enter the relevant model equations and constants. *
10 C Consult the User's Guide for details concerning the format for *
11 C entered equations and definition of symbols. *
12 C *
13 C 1. Symbol- Parameter symbols and model constants *
14 C 2. DiffEq- System differential equations *
15 C 3. Output- System output equations *
16 C 4. Varmod- Error variance model equations *
17 C 5. Covmod- Covariate model equations (ITS,MLEM) *
18 C 6. Popinit- Population parameter initial values (ITS,MLEM) *
19 C 7. Prior - Parameter mean and covariance values (ID,NPD,STS) *
20 C 8. Sparam- Secondary parameters *
21 C 9. Amat - System state matrix *
22 C *
23 C***************************************************************************
24 C#####################################################################C
25 Subroutine SYMBOL
26 Implicit None
27 Include 'globals.inc'
28 Include 'model.inc'
29 CC
30 C----------------------------------------------------------------C
31 C Enter as Indicated C
32 C----c-----------------------------------------------------------C
33 NDEqs = 66 ! Enter # of Diff. Eqs.
34 NSParam = 21 ! Enter # of System Parameters.
35 NVparam = 2 ! Enter # of Variance Parameters.
36 NSecPar = 0 ! Enter # of Secondary Parameters.
37 NSecOut = 0 ! Enter # of Secondary Outputs (not used).
38 Ieqsol = 1 ! Model type: 1 - DIFFEQ, 2 - AMAT, 3 - OUTPUT only.
39 Descr = ' simple PBPK of QC '
40 CC
41 C----------------------------------------------------------------C
42 C Enter Symbol for Each System Parameter (eg. Psym(1)='Kel') C
43 C----c-----------------------------------------------------------C
44 Psym(1)='Bmax_liver'
45 Psym(2)='Bmax_kidney'
46 Psym(3)='Bmax_heart'
47 Psym(4)='Bmax_muscle'
48 Psym(5)='Bmax_skin'
49 Psym(6)='Bmax_lung'
50 Psym(7)='Bmax_spleen'
```

```fortran
51 Psym(8)='Bmax_brain'
52 Psym(9)='Bmax_eye'
53 Psym(10)='Bmax_carcass'
54 Psym(11)='KD'
55 Psym(12)='KD2'
56 Psym(13)='kap'
57 Psym(14)='Kal'
58 Psym(15)='CL_int'
59 Psym(16)='F'
60 Psym(17)='ft'
61 Psym(18)='PS'
62 Psym(19)='PS2'
63 Psym(20)='PS3'
64 Psym(21)='PS4'
65 CC
66 C---------------------------------------------------------------C
67 C Enter Symbol for Each Variance Parameter {eg: PVsym(1)='Sigma'} C
68 C----c--------------------------------------------------------C
69 PVsym(1)='sigma'
70 PVsym(2)='intercept'
71 CC
72 C---------------------------------------------------------------C
73 C Enter Symbol for Each Secondary Parameter {eg: PSsym(1)='CLt'} C
74 C----c--------------------------------------------------------C
75 C---------------------------------------------------------------C
76 C---------------------------------------------------------------C
77 C
78 Return
79 End
80 C###########################################################################C
81 Subroutine DIFFEQ(T,X,XP)
82 Implicit None
83 Include 'globals.inc'
84 Include 'model.inc'
85 Real*8 T,X(MaxNDE),XP(MaxNDE)
86 Real*8 ka, F, Cl_kidney, Cl_liver, fu
87 Real*8 Bmax_liver, Kp_liver ,Kp_heart,KD3
88 Real*8 Kp_kidney, Bmax_kidney, Bmax_muscle,Kp_carcass
89 Real*8 Bmax_heart, Kp_muscle, Kp_skin, Bmax_skin,KD,KD2
90 Real*8 Q_liver, Q_heart, Q_gut, Q_kidney, Q_skin,Q_muscle
91 Real*8 Q_slow,Q_rapid, Q_blood,Q_carcass,ft_s,kal
92 Real*8 V_liver,V_kidney, V_muscle,V_blood,V_carcass,V_plasma
93 Real*8 V_heart,V_slow, V_rapid, V_skin, V_gut,Cl,ft_m
94 Real*8 Vmaxr,Kmr, Vmaxl,Kml,ft_h,ft_k,ft_l,fi,GFR,ft_c
95 Real*8 Q_lung, Q_spleen, Q_brain, Q_eye, Kp_lung, Kp_spleen
96 Real*8 Kp_brain, Kp_eye, V_lung,V_spleen, V_brain, V_eye
97 Real*8 V_artery, V_vein,Bmax_spleen,ft_b,ft_e,PS,PS2,PS3,PS4
98 Real*8 Bmax_lung,Bmax_eye,Bmax_brain,Bmax_carcass
99 Real*8 V_liver2,V_kidney2,V_heart2,V_muscle2,V_skin2,V_lung2
100 real*8 V_spleen2,V_brain2,CL_total
101 real*8 Kp_liver2,Kp_heart2,Kp_kidney2,Kp_carcass2,Kp_muscle2
102 real*8 Kp_skin2,Kp_spleen2,Kp_lung2,Kp_brain2, Kp_eye2
103 real*8 Kp_liver3,Kp_heart3,Kp_kidney3,Kp_carcass3,Kp_muscle3
```

```fortran
104 real*8 Kp_skin3,Kp_spleen3,Kp_lung3,Kp_brain3, Kp_eye3
105 CC
106 C------------------------------------------------------------------C
107 C Enter Differential Equations Below {e.g. XP(1) = -P(1)*X(1) } C
108 C----c-------------------------------------------------------------C
109 ! There is no Kp_brain, because it was permeability-limited
110 Bmax_liver=P(1)
111 Bmax_kidney=P(2)
112 Bmax_heart=P(3)
113 Bmax_muscle=P(4)
114 Bmax_skin=P(5)
115 Bmax_lung=P(6)
116 Bmax_spleen=P(7)
117 Bmax_brain=P(8)
118 Bmax_eye=P(9)
119 Bmax_carcass=P(10)
120 KD=P(11)
121 KD2=P(12)
122 ka=P(13)
123 kal=P(14)
124 !CL_total=P(15)
125 Cl=P(15)
126 Cl_kidney=1096
127 F=P(16)
128 ft_e=1.0
129 ft_k=1.0
130 ft_l=1.0
131 ft_m=P(17)
132 ft_h=1.0
133 ft_b=1.0
134 ft_s=P(17)
135 ft_c=1.0
136 PS=P(18)
137 PS2=P(19)
138 PS3=P(20)
139 PS4=P(21)
140 ! Tissue volume (mL/kg)
141 V_kidney=4.4*0.273
142 V_liver=25.7*0.161
143 V_heart=4.7*0.320
144 V_skin=37.1*0.382
145 V_muscle=400*0.118
146 V_lung=7.6*0.336
147 V_spleen=2.6*0.207
148 V_brain=20*0.162
149 V_eye=0.214
150 V_artery= 13.7
151 V_vein=32.1
152 V_carcass=452.1
153 V_kidney2=4.4*(1.0-0.273)
154 V_liver2=25.7*(1.0-0.161)
155 V_heart2=4.7*(1.0-0.320)
156 V_skin2=37.1*(1.0-0.382)
```

```
157 V_muscle2=400*(1.0-0.118)
158 V_lung2=7.6*(1.0-0.336)
159 V_spleen2=2.6*(1.0-0.207)
160 V_brain2=20*(1.0-0.162)
161 ! plasma flow was used to describe the flow rate to each tissues (mL/h/kg)
162 Q_kidney=484.6
163 Q_liver= 628.6
164 Q_heart= 110.8
165 Q_skin= 160.6
166 Q_muscle= 528.9
167 Q_carcass=401.5
168 Q_lung =2769
169 Q_spleen=138.6
170 Q_brain=315.7
171 Q_eye=0.0738
172 GFR=111
173 !Kp
174 fu=0.4
175 !dose 150mg-------------------------------------------------------------------
176 Kp_heart=F*(1+Bmax_heart/(KD+X(5)))
177 Kp_kidney=F*(1+Bmax_kidney/(KD+X(4)))
178 Kp_liver=F*(1+Bmax_liver/(KD+X(3)))
179 Kp_muscle=F*(1+Bmax_muscle/(KD2+X(7)))
180 Kp_skin=F*(1+Bmax_skin/(KD2+X(6)))
181 Kp_lung=F*(1+Bmax_lung/(KD+X(8)))
182 Kp_spleen=F*(1+Bmax_spleen/(KD+X(9)))
183 Kp_brain=F*(1+Bmax_brain/(KD+X(10)))
184 Kp_eye=F*(fu*(1+Bmax_eye/(KD2+fu*X(1))))
185 Kp_carcass=F*(fu*(1+Bmax_carcass/(KD+fu*X(1))))
186 !artery
187 XP(1)=(Q_lung*X(8)/fu+ka*X(2)-(CL_kidney+GFR)*X(1)*fu
188    -(Q_liver+Q_kidney+Q_heart+Q_skin*ft_s+
189    Q_muscle*ft_m+Q_spleen+Q_brain+Q_eye*ft_e+
190    Q_carcass*ft_c)*X(1))/V_artery
191 !vein
192 XP(14)=((Q_liver+Q_spleen)*X(3)/fu+Q_kidney*X(4)/fu+Q_heart*
193    X(5)/fu+Q_skin*ft_s*X(6)/fu+Q_muscle*ft_m*X(7)/fu
194    +Q_brain*ft_b*X(10)/fu
195    +Q_eye*ft_e*X(11)/Kp_eye+
196    Q_carcass*ft_c*X(12)/Kp_carcass-Q_lung*X(14))/V_vein
197 !oral plasma
198 XP(2)=-ka*X(2)
199 !oral liver
200 XP(13)=-kal*X(13)
201 !liver
202 XP(3)=(Q_liver*(X(1)-X(3)/fu)+Q_spleen*(X(9)/fu-X(3)/fu)
203    +kal*X(13)-PS*(X(3)-
204    X(15)/Kp_liver))/V_liver
205 XP(15)=(PS*(X(3)-X(15)/Kp_liver)-
206    Cl*X(15)/Kp_liver)/V_liver2
207 !kidney
208 XP(4)=(Q_kidney*(X(1)-X(4)/fu)-PS2*(X(4)-
209    X(16)/Kp_kidney))/V_kidney
```

210 XP(16)=PS2*(X(4)-X(16)/Kp_kidney)/V_kidney2
211 !heart
212 XP(5)=(Q_heart*(X(1)-X(5)/fu)-PS3*(X(5)-
213   X(17)/Kp_heart))/V_heart
214 XP(17)=PS3*(X(5)-X(17)/Kp_heart)/V_heart2
215 !skin
216 XP(6)=(Q_skin*ft_s*(X(1)-X(6)/fu)-PS4*(X(6)-
217   X(18)/Kp_skin))/V_skin
218 XP(18)=PS4*(X(6)-X(18)/Kp_skin)/V_skin2
219 !muscle
220 XP(7)=(Q_muscle*ft_m*(X(1)-X(7)/fu)-PS4*(X(7)-
221   X(19)/Kp_muscle))/V_muscle
222 XP(19)=PS4*(X(7)-X(19)/Kp_muscle)/V_muscle2
223 !lung
224 XP(8)=(Q_lung*(X(14)-X(8)/fu)-PS2*(X(8)-
225   X(20)/Kp_lung))/V_lung
226 XP(20)=PS2*(X(8)-X(20)/Kp_lung)/V_lung2
227 !spleen
228 XP(9)=(Q_spleen*(X(1)-X(9)/fu)-PS2*(X(9)-
229   X(21)/Kp_spleen))/V_spleen
230 XP(21)=PS2*(X(9)-X(21)/Kp_spleen)/V_spleen2
231 !brain
232 XP(10)=(Q_brain*(X(1)-X(10)/fu)-PS3*(X(10)-
233   X(22)/Kp_brain))/V_brain
234 XP(22)=PS3*(X(10)-X(22)/Kp_brain)/V_brain2
235 !eye
236 XP(11)=Q_eye*ft_e*(X(1)-X(11)/Kp_eye)/V_eye
237 !carcass
238 XP(12)=Q_carcass*ft_c*(X(1)-X(12)/Kp_carcass)/V_carcass
239 !dose
300mg--
----
240 Kp_heart2=F*(1+Bmax_heart/(KD+X(27)))
241 Kp_kidney2=F*(1+Bmax_kidney/(KD+X(26)))
242 Kp_liver2=F*(1+Bmax_liver/(KD+X(25)))
243 Kp_muscle2=F*(1+Bmax_muscle/(KD2+X(29)))
244 Kp_skin2=F*(1+Bmax_skin/(KD2+X(28)))
245 Kp_lung2=F*(1+Bmax_lung/(KD+X(30)))
246 Kp_spleen2=F*(1+Bmax_spleen/(KD+X(31)))
247 Kp_brain2=F*(1+Bmax_brain/(KD+X(32)))
248 Kp_eye2=F*(fu*(1+Bmax_eye/(KD2+fu*X(23))))
249 Kp_carcass2=F*(fu*(1+Bmax_carcass/(KD+fu*X(23))))
250 !artery
251 XP(23)=(Q_lung*X(30)/fu+ka*X(24)-(GFR+Cl_kidney)*X(23)*fu
252   -(Q_liver+Q_kidney+Q_heart+Q_skin*ft_s+
253   Q_muscle*ft_m+Q_spleen+Q_brain+Q_eye*ft_e+
254   Q_carcass*ft_c)*X(23))/V_artery
255 !vein
256 XP(36)=((Q_liver+Q_spleen)*X(25)/fu+Q_kidney*X(26)/fu+Q_heart*
257   X(27)/fu+Q_skin*ft_s*X(28)/fu+Q_muscle*ft_m*X(29)/fu
258   +Q_brain*ft_b*X(32)/fu
259   +Q_eye*ft_e*X(33)/Kp_eye2+
260   Q_carcass*ft_c*X(34)/Kp_carcass2-Q_lung*X(36))/V_vein

```
261 !oral plasma
262 XP(24)=-ka*X(24)
263 !oral liver
264 XP(35)=-kal*X(35)
265 !liver
266 XP(25)=(Q_liver*(X(23)-X(25)/fu)+Q_spleen*(X(31)/fu-X(25)/fu)
267   +kal*X(35)-PS*(X(25)-
268   X(37)/Kp_liver2))/V_liver
269 XP(37)=(PS*(X(25)-X(37)/Kp_liver2)-
270   Cl*X(37)/Kp_liver2)/V_liver2
271 !kidney
272 XP(26)=(Q_kidney*(X(23)-X(26)/fu)-PS2*(X(26)-
273   X(38)/Kp_kidney2))/V_kidney
274 XP(38)=PS2*(X(26)-X(38)/Kp_kidney2)/V_kidney2
275 !heart
276 XP(27)=(Q_heart*(X(23)-X(27)/fu)-PS3*(X(27)-
277   X(39)/Kp_heart2))/V_heart
278 XP(39)=PS3*(X(27)-X(39)/Kp_heart2)/V_heart2
279 !skin
280 XP(28)=(Q_skin*ft_s*(X(23)-X(28)/fu)-PS4*(X(28)-
281   X(40)/Kp_skin2))/V_skin
282 XP(40)=PS4*(X(28)-X(40)/Kp_skin2)/V_skin2
283 !muscle
284 XP(29)=(Q_muscle*ft_m*(X(23)-X(29)/fu)-PS4*(X(29)-
285   X(41)/Kp_muscle2))/V_muscle
286 XP(41)=PS4*(X(29)-X(41)/Kp_muscle2)/V_muscle2
287 !lung
288 XP(30)=(Q_lung*(X(36)-X(30)/fu)-PS2*(X(30)-
289   X(42)/Kp_lung2))/V_lung
290 XP(42)=PS2*(X(30)-X(42)/Kp_lung2)/V_lung2
291 !spleen
292 XP(31)=(Q_spleen*(X(23)-X(31)/fu)-PS2*(X(31)-
293   X(43)/Kp_spleen2))/V_spleen
294 XP(43)=PS2*(X(31)-X(43)/Kp_spleen2)/V_spleen2
295 !brain
296 XP(32)=(Q_brain*(X(23)-X(32)/fu)-PS3*(X(32)-
297   X(44)/Kp_brain2))/V_brain
298 XP(44)=PS3*(X(32)-X(44)/Kp_brain2)/V_brain2
299 !eye
300 XP(33)=Q_eye*ft_e*(X(23)-X(33)/Kp_eye2)/V_eye
301 !carcass
302 XP(34)=Q_carcass*ft_c*(X(23)-X(34)/Kp_carcass2)/V_carcass
303 !dose
600mg-----------------------------------------------------------------------
-----
304 Kp_heart3=F*(1+Bmax_heart/(KD+(49)))
305 Kp_kidney3=F*(1+Bmax_kidney/(KD+X(48)))
306 Kp_liver3=F*(1+Bmax_liver/(KD+X(47)))
307 Kp_muscle3=F*(1+Bmax_muscle/(KD2+X(51)))
308 Kp_skin3=F*(1+Bmax_skin/(KD2+X(50)))
309 Kp_lung3=F*(1+Bmax_lung/(KD+X(52)))
310 Kp_spleen3=F*(1+Bmax_spleen/(KD+X(53)))
311 Kp_brain3=F*(1+Bmax_brain/(KD+X(54)))
```

```
312 Kp_eye3=F*(fu*(1+Bmax_eye/(KD2+fu*X(45))))
313 Kp_carcass3=F*(fu*(1+Bmax_carcass/(KD+fu*X(45))))
314 !artery
315 XP(45)=(Q_lung*X(52)/fu+ka*X(46)-(GFR+CL_kidney)*X(45)*fu
316   -(Q_liver+Q_kidney+Q_heart+Q_skin*ft_s+
317   Q_muscle*ft_m+Q_spleen+Q_brain+Q_eye*ft_e+
318   Q_carcass*ft_c)*X(45))/V_artery
319 !vein
320 XP(58)=((Q_liver+Q_spleen)*X(47)/fu+Q_kidney*X(48)/fu+Q_heart*
321   X(49)/fu+Q_skin*ft_s*X(50)/fu+Q_muscle*ft_m*X(51)/fu
322   +Q_brain*ft_b*X(54)/fu
323   +Q_eye*ft_e*X(55)/Kp_eye3+
324   Q_carcass*ft_c*X(56)/Kp_carcass3-Q_lung*X(58))/V_vein
325 !oral plasma
326 XP(46)=-ka*X(46)
327 !oral liver
328 XP(57)=-kal*X(57)
329 !liver
330 XP(47)=(Q_liver*(X(45)-X(47)/fu)+Q_spleen*(X(53)/fu-X(47)/fu)
331   +kal*X(57)-PS*(X(47)-
332   X(59)/Kp_liver3))/V_liver
333 XP(59)=(PS*(X(47)-X(59)/Kp_liver3)-
334   Cl*X(59)/Kp_liver3)/V_liver2
335 !kidney
336 XP(48)=(Q_kidney*(X(45)-X(48)/fu)-PS2*(X(48)-
337   X(60)/Kp_kidney3))/V_kidney
338 XP(60)=PS2*(X(48)-X(60)/Kp_kidney3)/V_kidney2
339 !heart
340 XP(49)=(Q_heart*(X(45)-X(49)/fu)-PS3*(X(49)-
341   X(61)/Kp_heart3))/V_heart
342 XP(61)=PS3*(X(49)-X(61)/Kp_heart3)/V_heart2
343 !skin
344 XP(50)=(Q_skin*ft_s*(X(45)-X(50)/fu)-PS4*(X(50)-
345   X(62)/Kp_skin3))/V_skin
346 XP(62)=PS4*(X(50)-X(62)/Kp_skin3)/V_skin2
347 !muscle
348 XP(51)=(Q_muscle*ft_m*(X(45)-X(51)/fu)-PS4*(X(51)-
349   X(63)/Kp_muscle3))/V_muscle
350 XP(63)=PS4*(X(51)-X(63)/Kp_muscle3)/V_muscle2
351 !lung
352 XP(52)=(Q_lung*(X(58)-X(52)/fu)-PS2*(X(52)-
353   X(64)/Kp_lung3))/V_lung
354 XP(64)=PS2*(X(52)-X(64)/Kp_lung3)/V_lung2
355 !spleen
356 XP(53)=(Q_spleen*(X(45)-X(53)/fu)-PS2*(X(53)-
357   X(65)/Kp_spleen3))/V_spleen
358 XP(65)=PS2*(X(53)-X(65)/Kp_spleen3)/V_spleen2
359 !brain
360 XP(54)=(Q_brain*(X(45)-X(54)/fu)-PS3*(X(54)-
361   X(66)/Kp_brain3))/V_brain
362 XP(66)=PS3*(X(54)-X(66)/Kp_brain3)/V_brain2
363 !eye
364 XP(55)=Q_eye*ft_e*(X(45)-X(55)/Kp_eye3)/V_eye
```

```fortran
365 !carcass
366 XP(56)=Q_carcass*ft_c*(X(45)-X(56)/Kp_carcass3)/V_carcass
367 C-----------------------------------------------------------------C
368 C-----------------------------------------------------------------C
369 C
370 Return
371 End
372 C#################################################################C
373 Subroutine OUTPUT(Y,T,X)
374 Implicit None
375 Include 'globals.inc'
376 Include 'model.inc'
377 Real*8 Y(MaxNOE),T,X(MaxNDE)
378 Real*8 Bmax_liver, Kp_liver ,Kp_heart
379 Real*8 Kp_kidney, Bmax_kidney, Bmax_muscle,Bmax_blood,fu
380 Real*8 Bmax_heart, Kp_muscle, Kp_skin, Bmax_skin,KD
381 Real*8 Q_liver, Q_heart, Q_gut, Q_kidney, Q_skin,Q_muscle
382 Real*8 Q_eye,Q_slow,Q_rapid, Q_blood,Q_carcass,Kp_blood
383 Real*8 V_liver,V_kidney, V_muscle,V_blood,V_carcass,V_plasma
384 Real*8 V_heart,V_slow, V_rapid, V_skin, V_gut,Cl
385 Real*8 Vmaxr,Kmr, Vmaxl,Kml
386 Real*8 Vl_liver,Vl_kidney,Vl_heart,Vl_skin,Vl_muscle,Vl_carcass
387 Real*8 At_liver,At_kidney,At_heart,At_skin,At_muscle,At_carcass
388 Real*8 fnc,fnl,N1,N2,EN1,EN2,Pn,PD1,PD2,D1o,D1i,D2o,D2i
389 Real*8 V_liver2,V_kidney2,V_heart2,V_muscle2,V_skin2,V_lung2
390 real*8 V_spleen2,V_brain2
391 Real*8 V_lung
392 real*8 V_spleen,V_brain
393 CC
394 C-----------------------------------------------------------------C
395 C Enter Output Equations Below {e.g. Y(1) = X(1)/P(2) } C
396 C----c------------------------------------------------------------C
397 Y(1)=X(1)
398 Y(2)=X(23)
399 Y(3)=X(45)
400 C-----------------------------------------------------------------C
401 C-----------------------------------------------------------------C
402 C
403 Return
404 End
405 C#################################################################C
406 Subroutine VARMOD(V,T,X,Y)
407 Implicit None
408 Include 'globals.inc'
409 Include 'model.inc'
410 Real*8 V(MaxNOE),T,X(MaxNDE),Y(MaxNOE)
411 CC
412 C-----------------------------------------------------------------C
413 C Enter Variance Model Equations Below C
414 C {e.g. V(1) = (PV(1) + PV(2)*Y(1))**2 } C
415 C----c------------------------------------------------------------C
416 V(1) = (PV(2) + PV(1)*Y(1))**2
417 V(2) = (PV(2) + PV(1)*Y(2))**2
```

```fortran
418 V(3) = (PV(2) + PV(1)*Y(3))**2
419 C----------------------------------------------------------------C
420 C----------------------------------------------------------------C
421 C
422 Return
423 End
424 C###############################################################C
425 Subroutine COVMOD(Pmean, ICmean, PC)
426 C Defines any covariate model equations (MLEM, ITS)
427 Implicit None
428 Include 'globals.inc'
429 Include 'model.inc'
430 Real*8 PC(MaxNCP)
431 Real*8 Pmean(MaxNSP+MaxNDE), ICmean(MaxNDE)
432 CC
433 C----------------------------------------------------------------C
434 C Enter # of Covariate Parameters C
435 C----c-----------------------------------------------------------C
436 NCparam = 0 ! Enter # of Covariate Parameters.
437 CC
438 C----------------------------------------------------------------C
439 C Enter Symbol for Covariate Params {eg: PCsym(1)='CLRenal'} C
440 C----c-----------------------------------------------------------C
441 CC
442 C----------------------------------------------------------------C
443 C For the Model Params. that Depend on Covariates Enter the Equation C
444 C {e.g. Pmean(1) = PC(1)*R(2) } C
445 C----c-----------------------------------------------------------C
446 C----------------------------------------------------------------C
447 C----------------------------------------------------------------C
448 C
449 Return
450 End
451 C###############################################################C
452 Subroutine POPINIT(PmeanI,ICmeanI,PcovI,ICcovI, PCI)
453 C Initial parameter values for population program parameters (ITS, MLEM)
454 Implicit None
455 Include 'globals.inc'
456 Include 'model.inc'
457 Integer I,J
458 Real*8 PmeanI(MaxNSP+MaxNDE), ICmeanI(MaxNDE)
459 Real*8 PcovI(MaxNSP+MaxNDE,MaxNSP+MaxNDE), ICcovI(MaxNDE,MaxNDE)
460 Real*8 PCI(MaxNCP)
461 CC
462 C----------------------------------------------------------------C
463 C Enter Initial Values for Population Means C
464 C { e.g. PmeanI(1) = 10.0 } C
465 C----c-----------------------------------------------------------C
466 CC
467 C----------------------------------------------------------------C
468 C Enter Initial Values for Pop. Covariance Matrix (Lower Triang.) C
469 C { e.g. PcovI(2,1) = 0.25 } C
470 C----c-----------------------------------------------------------C
```

```fortran
471 CC
472 C----------------------------------------------------------------C
473 C Enter Values for Covariate Model Parameters C
474 C { e.g. PCI(1) = 2.0 } C
475 C----c-----------------------------------------------------------C
476 C----------------------------------------------------------------C
477 C----------------------------------------------------------------C
478 C
479 Return
480 End
481 C####################################################################C
482 Subroutine PRIOR(Pmean,Pcov,ICmean,ICcov)
483 C Parameter mean and covariance values for MAP estimation (ID,NPD,STS)
484 Implicit None
485 Include 'globals.inc'
486 Include 'model.inc'
487 Integer I,J
488 Real*8 Pmean(MaxNSP+MaxNDE), ICmean(MaxNDE)
489 Real*8 Pcov(MaxNSP+MaxNDE,MaxNSP+MaxNDE), ICcov(MaxNDE,MaxNDE)
490 CC
491 C----------------------------------------------------------------C
492 C Enter Nonzero Elements of Prior Mean Vector C
493 C { e.g. Pmean(1) = 10.0 } C
494 C----c-----------------------------------------------------------C
495 CC
496 C----------------------------------------------------------------C
497 C Enter Nonzero Elements of Covariance Matrix (Lower Triang.) C
498 C { e.g. Pcov(2,1) = 0.25 } C
499 C----c-----------------------------------------------------------C
500 C----------------------------------------------------------------C
501 C----------------------------------------------------------------C
502 C
503 Return
504 End
505 C####################################################################C
506 Subroutine SPARAM(PS,P,IC)
507 Implicit None
508 Include 'globals.inc'
509 Real*8 PS(MaxNSECP), P(MaxNSP+MaxNDE), IC(MaxNDE)
510 CC
511 C----------------------------------------------------------------C
512 C Enter Equations Defining Secondary Paramters C
513 C { e.g. PS(1) = P(1)*P(2) } C
514 C----c-----------------------------------------------------------C
515 C----------------------------------------------------------------C
516 C----------------------------------------------------------------C
517 C
518 Return
519 End
520 C####################################################################C
521 Subroutine AMAT(A)
522 Implicit None
523 Include 'globals.inc'
```

```fortran
524 Include 'model.inc'
525 Integer I,J
526 Real*8 A(MaxNDE,MaxNDE)
527 DO I=1,Ndeqs
528 Do J=1,Ndeqs
529 A(I,J)=0.0D0
530 End Do
531 End Do
532 CC
533 C----------------------------------------------------------------C
534 C Enter non zero elements of state matrix {e.g. A(1,1) = -P(1) } C
535 C----c-----------------------------------------------------------C
536 C----------------------------------------------------------------C
537 C----------------------------------------------------------------C
538 C
539 Return
540 End
541 C################################################################C
```